NANO · MICRO small
www.small-journal.com

A Safe, Fibrosis-Mitigating, and Scalable Encapsulation Device Supports Long-Term Function of Insulin-Producing Cells

*Wanjun Liu, James A. Flanders, Long-Hai Wang, Qingsheng Liu, Daniel T. Bowers, Kai Wang, Alan Chiu, Xi Wang, Alexander U. Ernst, Kaavian Shariati, Julia S. Caserto, Benjamin Parker, Daqian Gao, Mitchell D. Plesser, Lars G. Grunnet, Claude Rescan, Rodrigo Pimentel Carletto, Louise Winkel, Juan M. Melero-Martin, and Minglin Ma**

Encapsulation and transplantation of insulin-producing cells offer a promising curative treatment for type 1 diabetes (T1D) without immunosuppression. However, biomaterials used to encapsulate cells often elicit foreign body responses, leading to cellular overgrowth and deposition of fibrotic tissue, which in turn diminishes mass transfer to and from transplanted cells. Meanwhile, the encapsulation device must be safe, scalable, and ideally retrievable to meet clinical requirements. Here, a durable and safe nanofibrous device coated with a thin and uniform, fibrosis-mitigating, zwitterionically modified alginate hydrogel for encapsulation of islets and stem cell-derived beta (SC-β) cells is reported. The device with a configuration that has cells encapsulated within the cylindrical wall, allowing scale-up in both radial and longitudinal directions without sacrificing mass transfer, is designed. Due to its facile mass transfer and low level of fibrotic reactions, the device supports long-term cell engraftment, correcting diabetes in C57BL6/J mice with rat islets for up to 399 days and SCID-beige mice with human SC-β cells for up to 238 days. The scalability and retrievability in dogs are further demonstrated. These results suggest the potential of this new device for cell therapies to treat T1D and other diseases.

1. Introduction

Type 1 diabetes (T1D) is an auto-immune disease characterized by a loss of β cells.[1–3] Patients must frequently monitor their blood glucose levels and undergo insulin therapy to maintain the blood glucose in a healthy range. This task is not only stressful but omnipresent for patients at every point of time in their lives. Current therapies involve either daily injections of insulin or the use of an insulin pump to suit a patient's needs.[4–6] Other devices such as Continuous Glucose Monitors offer more information and peace of mind to patients, but nonetheless require extensive input and effort from patients.[7] Alternatively, transplantation of insulin-producing cells represents a promising curative treatment for type 1 diabetes by providing patients with cells that perform the functions they have lost.[8,9] Notably, more than 1500 patients have been treated with human islet transplantation and

W. Liu, L.-H. Wang, Q. Liu, D. T. Bowers, A. Chiu, X. Wang, A. U. Ernst, K. Shariati, J. S. Caserto, B. Parker, D. Gao, M. D. Plesser, M. Ma
Department of Biological and Environmental Engineering
Cornell University
Ithaca, NY 14853, USA
E-mail: mm826@cornell.edu

W. Liu
Key Laboratory of Textile Science & Technology
Ministry of Education
College of Textiles
Donghua University
Shanghai 201620, China

J. A. Flanders
Department of Clinical Sciences
Cornell University
Ithaca, NY 14853, USA

The ORCID identification number(s) for the author(s) of this article can be found under https://doi.org/10.1002/smll.202104899.

DOI: 10.1002/smll.202104899

K. Wang, J. M. Melero-Martin
Department of Cardiac Surgery
Boston Children's Hospital
Boston, MA 02115, USA

K. Wang, J. M. Melero-Martin
Department of Surgery
Harvard Medical School
Boston, MA 02115, USA

J. S. Caserto
Robert Frederick Smith School of Chemical and Biomolecular Engineering
Cornell University
Ithaca, NY 14853, USA

L. G. Grunnet, C. Rescan, R. Pimentel Carletto, L. Winkel
Stem Cell Delivery and Pharmacology
Novo Nordisk A/S, Måløv 2760, Denmark

J. M. Melero-Martin
Harvard Stem Cell Institute
Cambridge, MA 02138, USA

achieved clinical success since 2000.[8] However, limited patients benefit from islet transplantation due to donor shortage and the requirement of chronic immune suppression.[10]

Cell encapsulation,[1,2,4,5,11] designed to establish an immunological barrier against the host to protect transplanted cells while allowing free transfer of glucose, insulin, and essential nutrients, has been widely investigated for immunosuppression-free cell replacement therapies for T1D. This approach has become particularly attractive in recent years due to the capability of generating a limitless supply of stem cell-derived beta (SC-β) cells,[12] relieving the cadaveric donor tissue limitations and benefiting much broader patient populations. However, developing a clinically feasible, long-term functional cell encapsulation device is a significant, unmet challenge.[1,2,4] An arduous obstacle is the foreign body response against the encapsulation device, which leads to cellular overgrowth and fibrotic deposition, resulting in diminished mass transfer and graft failure.[1,13,14] For example, the ViaCyte device[15] and the Beta-Air device,[16] the two most advanced devices in the field, although promising in preventing allo- and auto-immune responses, failed to provide any clinical benefit or long-term cell function due to compromised mass transfer caused by foreign body response and fibrotic reactions.[14,17–19]

Efforts have been made to tackle the challenge of foreign body responses, especially for the most used encapsulation material – alginate hydrogel.[20–22] For example, combinational approaches have been employed to identify advanced alginate derivatives from 774 chemical modifications. Three "hits" substantially reduced cellular overgrowth on implanted alginate microcapsules in both mice and non-human primates.[21,23] Our group developed fibrosis-mitigating alginate microcapsules using a rational design approach. We modified alginate with zwitterionic functional groups[18] known for their biofouling-resistant properties[24] and observed reproducible and robust reduction of cellular overgrowth in various models, including mice, dogs, and pigs. We also demonstrated that microcapsules made of one of the zwitterionically modified alginates encapsulating rat islets enabled long-term diabetes correction for up to 200 days in immunocompetent mice. Although these results are promising, our inability to reliably retrieve all transplanted microcapsules,[18,25] and the intrinsic weakness of hydrogel materials[26] raise safety concerns for clinical applications. These concerns merit particular consideration when SC-β cells are used due to the potential risk of nontarget cells.[14,22,27,28]

To mitigate the safety concerns while leveraging the superior biocompatibility of the zwitterionic alginates, here we report a safe, hypo-immunoreactive, islet encapsulation, long-term-functional device (SHIELD) for delivery of islets and human SC-β cells. SHIELD has several unique features which bestow translational advantages. First, we designed a concentric configuration where cells are encapsulated within the cylindrical wall, allowing scale-up in both radial and longitudinal directions without sacrificing diffusion distance or mass transfer. Second, the strong and robust nanofibrous membrane with tunable, interconnected pore structure provided excellent mass transfer while ensuring safety. Third, we developed an innovative "in-out crosslinking" strategy to coat the nanofibrous membrane with a thin, uniform, controllable and stable layer of alginate hydrogel. Lastly, the zwitterionically modified alginate[18] mitigated fibrotic reactions and endowed SHIELD with long-term function. Imaging, tensile, and peeling tests indicated that the "in-out crosslinking" resulted in an interpenetrating composite structure between the nanofibers and the alginate coating, exhibiting both high tensile strength and strong interfacial adhesion. In vitro and in vivo optimizations culminated in a device capable of preventing cell escape of encapsulated cells and penetration of host cells, while supporting normal functions of encapsulated cells. Facilitated by its facile mass transfer and resistance to fibrotic reactions, SHIELD exhibited long-term restoration of normoglycemia (up to 399 days) in immunocompetent diabetic mice when encapsulated with rat islets. More importantly, SHIELD encapsulating human SC-β cells corrected diabetes in SCID-Beige mice shortly after implantation for up to 238 days. Lastly, scalability and ease of retrieval were achieved and demonstrated in dogs.

2. Results

2.1. Design and Fabrication of SHIELD with Safety, Scalability, and Biocompatibility

We considered several criteria in designing SHIELD. To maximize scalability, we adopted a concentric geometry and encapsulated cells in the cylindrical wall where the loading capacity is decoupled from the diffusion distance (**Figure 1**a–e), allowing scale-up in both longitudinal and radial directions. For safety, we used an electrospun nylon nanofiber membrane as a barrier which is not only mechanically robust but also has tunable pore structures (Figure 1f), allowing us to balance safety (i.e., prevention of cell escape) and function (i.e., facile mass transfer). To attain good biocompatibility, we coated the device with a zwitterionically modified alginate capable of mitigating fibrotic reactions (Figure 1d,g,h), thus maintaining facile mass transfer and enabling long-term function of encapsulated cells.

To realize the concentric configuration, we first coated an inner nanofibrous tube with cell-laden alginate hydrogel (Figure 1b,c), then inserted it into another outer nanofibrous tube (alginate-coated), followed by thermal sealing using a custom-designed thermo cutting device (Figure 1d,e and Figure S1, Supporting Information). It should be noted that the quality of alginate coating is super crucial to the performance of cell encapsulation devices. Previously reported methods such as impregnating porous membranes with alginate precursors and subsequent crosslinking often had poor control over uniformity and thickness.[28] Here we developed a new method to achieve uniform coating with controllable thickness (Figure 1d). Specifically, a one-end sealed, dry nanofibrous tube was first dipped into alginate precursors to facilitate the alginate penetration into the nanofibrous wall. Subsequently, a crosslinking solution was injected into the lumen from the open end so that crosslinkers could uniformly diffuse through the interconnected pores of the nanofibrous wall and gradually crosslink the alginate from the inside to the outside (we term this process as "in-out crosslinking"), resulting in a layer of uniform and

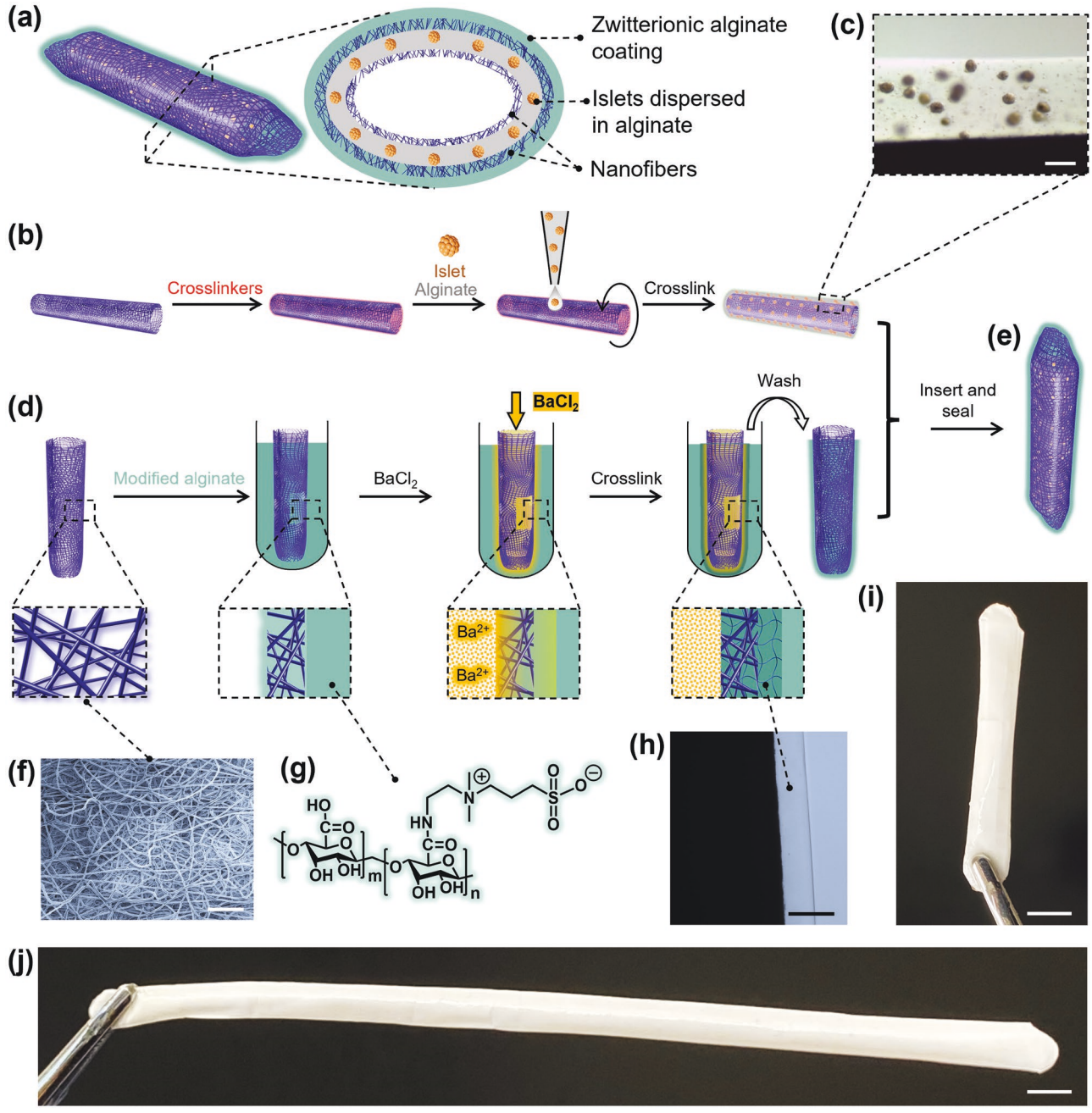

Figure 1. Design and fabrication of SHIELD. a) A schematic diagram showing SHIELD consisting of an inner nanofibrous tube and an outer nanofibrous tube. The inner nanofibrous tube keeps the clusters of insulin-producing cells around the inner surface of the outer nanofibrous tube and thus maintains a short diffusion distance. The outer nanofibrous tube is coated with zwitterionic alginate hydrogel for fibrosis mitigation. b–e) Fabrication of SHIELD: b) a schematic diagram showing the process of loading islets/alginate mixture onto the outer surface of the inner nanofibrous tube; c) a representative image of the inner nanofibrous tube loaded with islets (the black area is nanofiber membrane), scale bar, 200 µm; d) a schematic diagram of the "in-out crosslinking" method for fabricating the outer nanofibrous tube, which generates a uniform and stable coating with controllable thickness; e) SHIELD was achieved after inserting the inner nanofibrous tube (loaded with islets) to the coated outer nanofibrous tube followed by thermo sealing. f) An SEM image showing the interconnected porous structure of nanofiber membranes, scale bar, 20 µm. g) The chemical structure of zwitterionic alginate. h) An optical image showing the uniformity of the coated alginate hydrogel fabricated by the "in-out crosslinking" method (the black area is nanofiber membrane; the transparent area is alginate hydrogel), scale bar, 200 µm. i) A representative image of rodent-size SHIELDs (length ≈ 2.5 cm), scale bar, 5 mm. j) A representative image of long SHIELDs (length ≈ 10 cm), scale bar, 5 mm.

smooth hydrogel coating (Figure 1h and Figure S2a, Supporting Information). The coating thickness could be controlled by adjusting the diffusion time. For example, the coating thickness increased from ≈65 ± 15 to ≈188 ± 21 µm when the diffusion time was extended from 30 to 210 s (Figure S2b–f, Supporting Information). After washing away uncrosslinked alginate,

the coated tube was resubmerged in crosslinking buffer to further crosslink and improve the mechanical properties of the hydrogel coating. Importantly, the "in-out crosslinking" is applicable for devices with various lengths and diameters (Figure 1i,j) and scalable to clinically relevant capacities. Additionally, the sterile coated nanofibrous tubes could be prepared in advance and thus available off the shelf. Furthermore, the lumen of the inner tube could be filled with a kink-preventing template for long devices, necessary for scale-up and further discussed in the dog study.

2.2. The "In-Out Crosslinking" Method Leads to Robust Alginate Coating

Another advantage of the "in-out crosslinking" is that the interconnected pores of the nanofibrous membranes are occupied by alginate hydrogels, enabling a robust mechanical interlock between the coated hydrogel and the membrane, and thus good coating stability. To verify the interlock, we first performed tensile tests (**Figure 2**a–d). Dip-coated membranes without interlocked interaction (see details in the Experimental Section) were

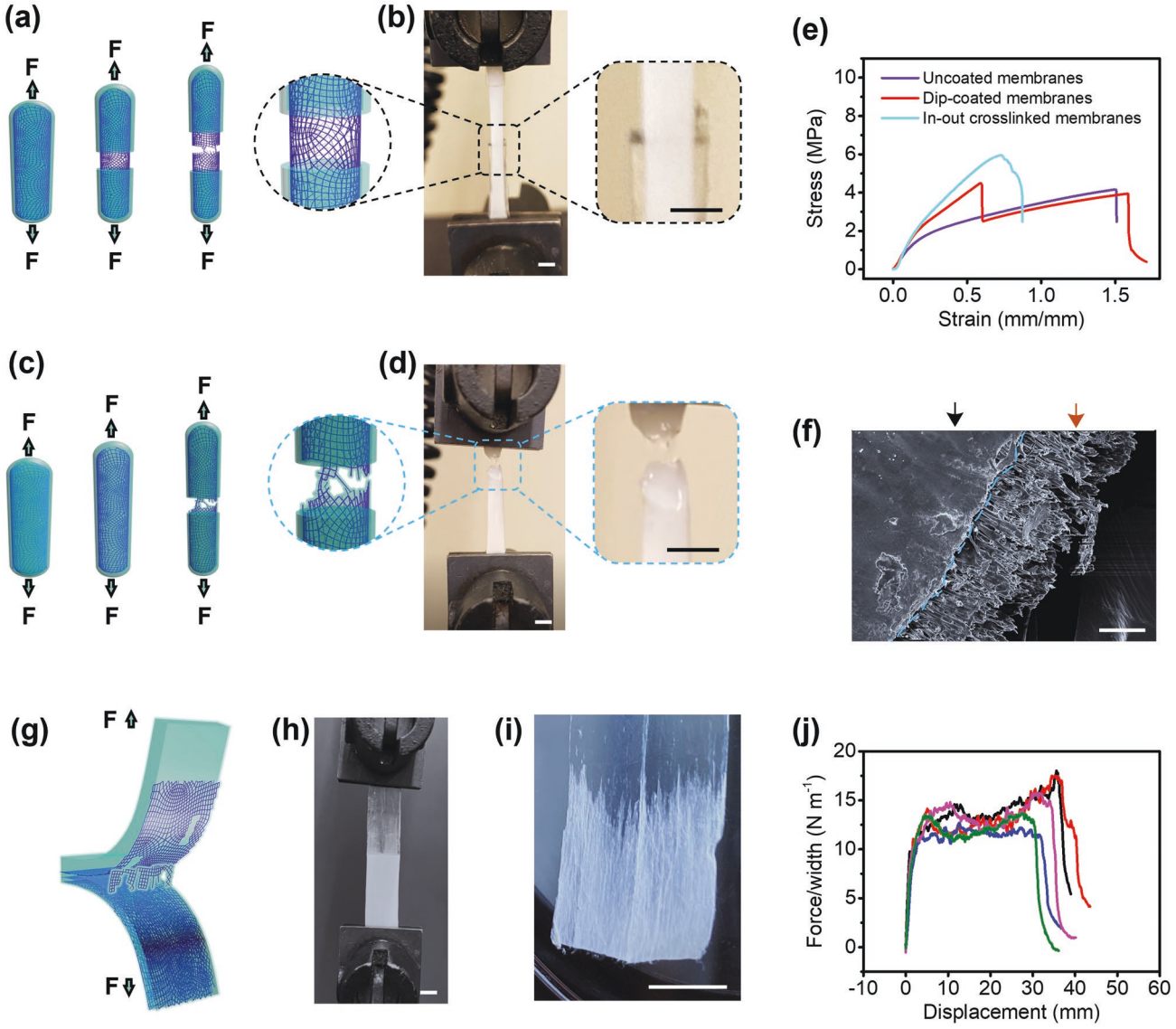

Figure 2. The "in-out crosslinking" method leads to robust alginate coating. a–d) Tensile test for dip-coated membranes and "in-out crosslinked" membranes: a,b) delamination between alginate hydrogel and nanofiber membrane was observed for dip-coated membranes; c,d) "in-out crosslinked" membranes exhibited an excellent integration between alginate hydrogel and the nanofiber membrane during the tensile test, scale bars, 5 mm. e) Stress–strain curves for uncoated membranes, dip-coated membranes, and "in-out crosslinked" membranes. f) An SEM image showing the interpenetration between alginate and nanofibers for "in-out crosslinked" membranes, scale bar, 20 µm (The black arrow and red arrow point to the alginate surface and the composite of alginate and nanofibers, respectively. While the dashed line indicates the boundary between pure alginate and nanofibers). g–j) Peeling test for "in-out crosslinked" membranes: g–i) remaining nanofibers on the hydrogel after the peeling test verified the strong coating adhesion enabled by the "in-out crosslinking" method; j) force/width as a function of displacement for the peeling test, scale bars, 5 mm.

prepared as a control. It is noted that the thickness of alginate was neglected for the convenience of comparison. According to the stress-strain curve, dip-coated membranes exhibited two breaking points (Figure 2e). At the strain of ≈0.56 mm mm^{-1}, the first stress drop represented the break of alginate coating. Further elongation resulted in apparent delamination between coated alginate and nanofiber membrane (Figure 2a,b and Movie S1, Supporting Information), which was not observed for the "in-out crosslinked" membranes (Figure 2c,d and Movie S2, Supporting Information). In addition, the stress and strain at the second breaking point were in agreement with those of uncoated nanofiber membranes (Figure S3a,b, Supporting Information), further verifying that there was no interlocked interaction for dip-coated membranes. On the contrary, only one breaking point was observed for the "in-out crosslinked" membranes, exhibiting a larger Young's modulus than that of dip-coated membranes (Figure S3c, Supporting Information). Furthermore, the tensile strength of the "in-out crosslinked" membranes was significantly higher than that of dip-coated membranes at the first breaking point (Figure S3d, Supporting Information). The tensile strain of the "in-out crosslinked" membranes was between the two breaking points for dip-coated membranes (Figure S3e,f, Supporting Information). These results indicate that the "in-out crosslinking" resulted in the formation of an integrated nanofiber–hydrogel composite. To view the structure of "in-out crosslinked" membranes, scanning electron microscopy (SEM) was used to image the cross-section of lyophilized samples. As expected, the interpenetration between alginate and nylon nanofibers was observed (Figure 2f). Lastly, to directly measure adhesion between the hydrogel coating and the nanofibrous membrane, we performed peeling tests (Figure 2g–j). Results showed that the adhesion between coated hydrogel and nanofiber membrane was 13.1 ± 1.5 N m^{-1} (Figure 2j), which was remarkable given the intrinsically weak mechanical properties of alginate hydrogels. The strong adhesion was also evidenced by the existence of residual nanofibers on the hydrogel after peeling tests (Figure 2h,i and Movie S3, Supporting Information). Taken together, it was clear that the new "in-out crosslinking" method resulted in a uniform and robust alginate coating with controllable thickness and strong adhesion.

2.3. Optimize the Pore Size by Balancing Safety and Mass Transfer

Next, we sought to optimize mass transfer while ensuring that SHIELD could confine encapsulated cells and prevent cell escape. Devices with average pore sizes ranging from 0.15 to 1.67 μm were fabricated by adjusting the nanofiber diameter (**Figure 3**a and Figure S4a–j, Supporting Information). To investigate cell escape, GFP expressing cells (NIH3T3/GFP) dispersed in 60 μL fibrin/gelatin hydrogels at a density of 1.0 million mL^{-1} were encapsulated in the device, cultured, and monitored for up to 2 weeks. NIH3T3/GFP cells were used mainly for the convenience of imaging and detecting, which allowed us to promptly detect escaped cells on opaque SHIELDs by fluorescent imaging. In addition, the inherent proliferating and migrating properties of NIH3T3/GFP cells enabled us to quickly evaluate the capability of preventing cell escape. Fibrin gel, which could be degraded by NIH3T3/GFP cells in 2–3 days, was used as the matrix to allow for free cell growth and migration. Both uncoated and coated devices were evaluated. Cell escape was only observed for the uncoated device with a pore size of 1.67 μm, while devices with the other pore sizes completely confined the cells (Figure 3b, Figures S5a–t, S6a–t, and S7, Supporting Information). For the 1.67 μm pore size, two out of five devices failed to confine the cells since day 5 and the remainder failed between day 7 and day 10 (Figure S7a–k, Supporting Information).

Interestingly, when the devices were coated with alginate hydrogel, even those with the largest pore size of 1.67 μm could prevent cell escape (Figures S6a–v and S7l–v, Supporting Information), suggesting that the formation of alginate hydrogel in the interconnected pores of nanofiber membranes could prevent the cells from escaping. Importantly, substantial and crowded cells were observed in both coated and uncoated devices for all the pore sizes investigated (Figures S5u–y and S6u–y, Supporting Information). Furthermore, presto blue and Live/Dead staining confirmed that cells remained viable and proliferated normally in the coated devices, verifying that the mass transfer of *SHIELD* was sufficient for encapsulated cells (Figure 3c,d). Lastly, we implanted empty uncoated devices into the intraperitoneal cavity of C57BL6/J mice for two weeks to assess the fibrotic reaction and penetration of host cells. Histological images (Figure 3e–h and Figure S4k–o, Supporting Information) revealed that the 1.67 μm uncoated device allowed extensive cell penetration into the nanofibrous membrane. While the other uncoated devices had minimal (for 0.67 and 1.05 μm devices) or no cell penetration (for 0.15 and 0.38 μm devices). In addition, the thickness of the fibrotic layer on the device first increased and then decreased when the average pore size was changed from 0.15 to 1.67 μm, with the peak at 0.67 μm (Figure 3i). Furthermore, tissue adhesion occurred to uncoated devices with all pore sizes, with the highest frequency for 0.38 μm devices (Figure 3j). To maximize mass transfer while avoiding cell escape and cell penetration, we chose the device with 1.05 μm average pore size in the following in vivo investigations. Particularly, mass transfer was the primary consideration as 1.05 μm was the largest pore size exhibiting minimal cell penetration in vivo. In addition, we were also motivated by the results that all alginate coated devices prevented cell escape in vitro. Therefore, we believed 1.05 μm coated devices might be capable of preventing cell penetration in vivo. As expected, no cell penetration was observed for 1.05 μm coated devices in vivo, as shown in the following investigations.

2.4. Stable Zwitterionic Alginate Coating Results in Superior Biocompatibility

Alginate hydrogel is a commonly used material for cell encapsulation. However, its inadequate biocompatibility remains a challenge. We previously developed zwitterionically modified alginates and showed reproducible and robust reduction of cellular overgrowth on microcapsules in mice, dogs, and pigs. Here we applied one of the zwitterionic alginates, sulfobetaine-modified alginate (SB-alginate), to SHIELD as a thin and uniform coating

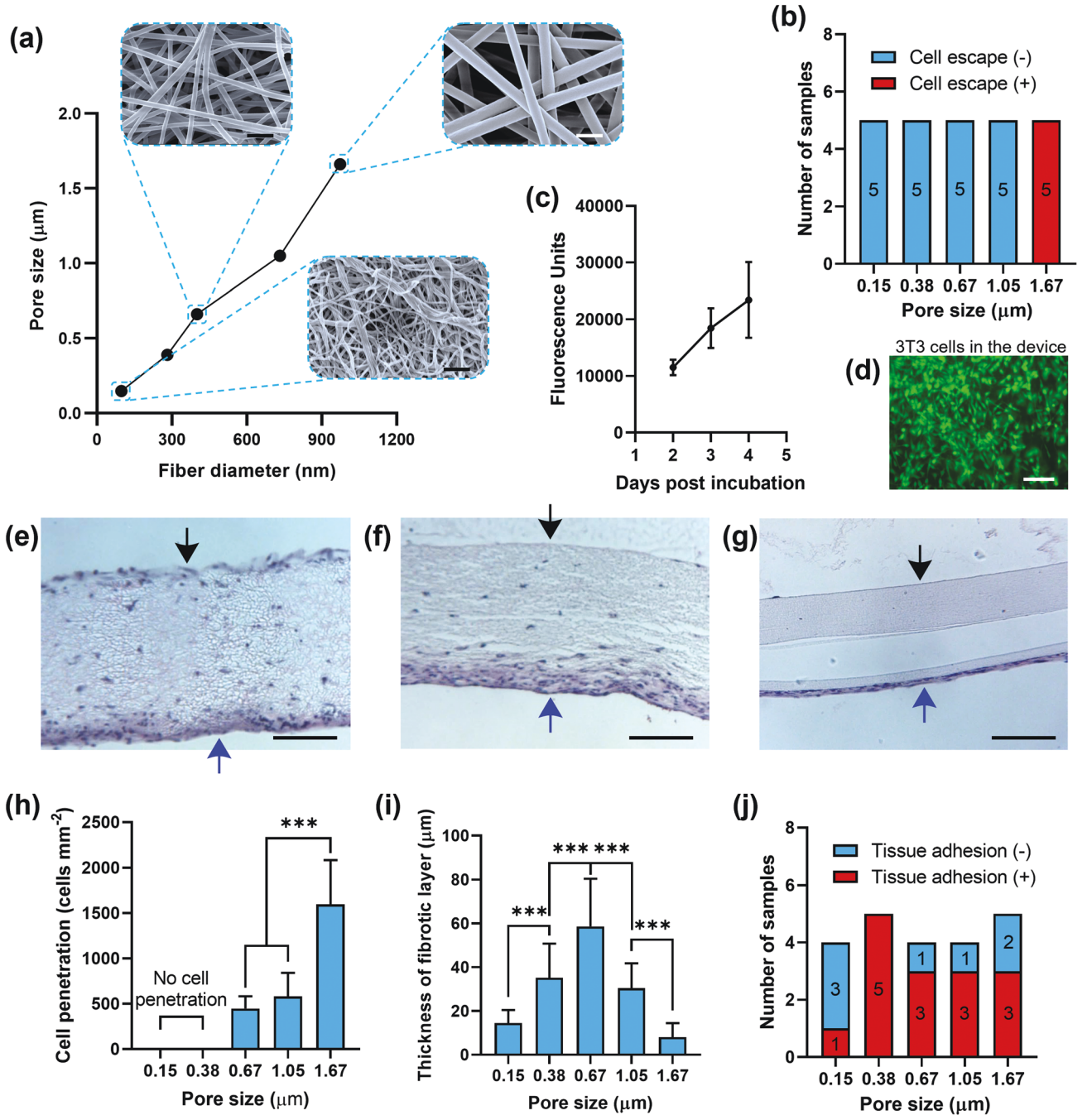

Figure 3. Optimization of the pore size by balancing safety and mass transfer. a) Pore size as a function of fiber diameter, scale bars, 2 μm. b) Number of samples having cell escape on day 14 for uncoated devices with different pore sizes (average pore size: 0.15, 0.38, 0.67, 1.05, and 1.67 μm). c) Fluorescence units as a function of days post incubation for the presto blue test. d) A Live/Dead image of NIH3T3 cells inside a coated device after 2-day incubation, scale bar, 200 μm. e–g) H&E images of uncoated devices after 14-day in vivo test in the intraperitoneal space of healthy C57BL6/J mice (n = 4 or 5 for each pore size, blue arrows point to the outer surface of devices, while black arrows point to the inner surface), scale bars, 200 μm: e) 1.67 μm; f) 0.67 μm; g) 0.15 μm. h–j) Quantification of h) cell penetration, i) thickness of fibrotic layer, and j) number of samples having tissue adhesion for uncoated devices with different pore sizes.

to improve its biocompatibility. By seeding NIH3T3/GFP cells on the outer surface of coated devices, we confirmed that modified alginate indeed performed better in preventing cell attachment compared to unmodified SLG100 alginate (**Figure 4**a,b,g). To obtain the best coating stability in vivo, we used the "in-out crosslinking" method, and tested alginate with three different ratios between SB-alginate and unmodified high molecular weight alginate SLG100 (i.e., SB-alginate:SLG100 = 7:3, 5:5, 3:7). Neat SLG100 alginate coating (or 0:10) was included as a control. After intraperitoneal implantation in C57BL6/J mice for 2 and

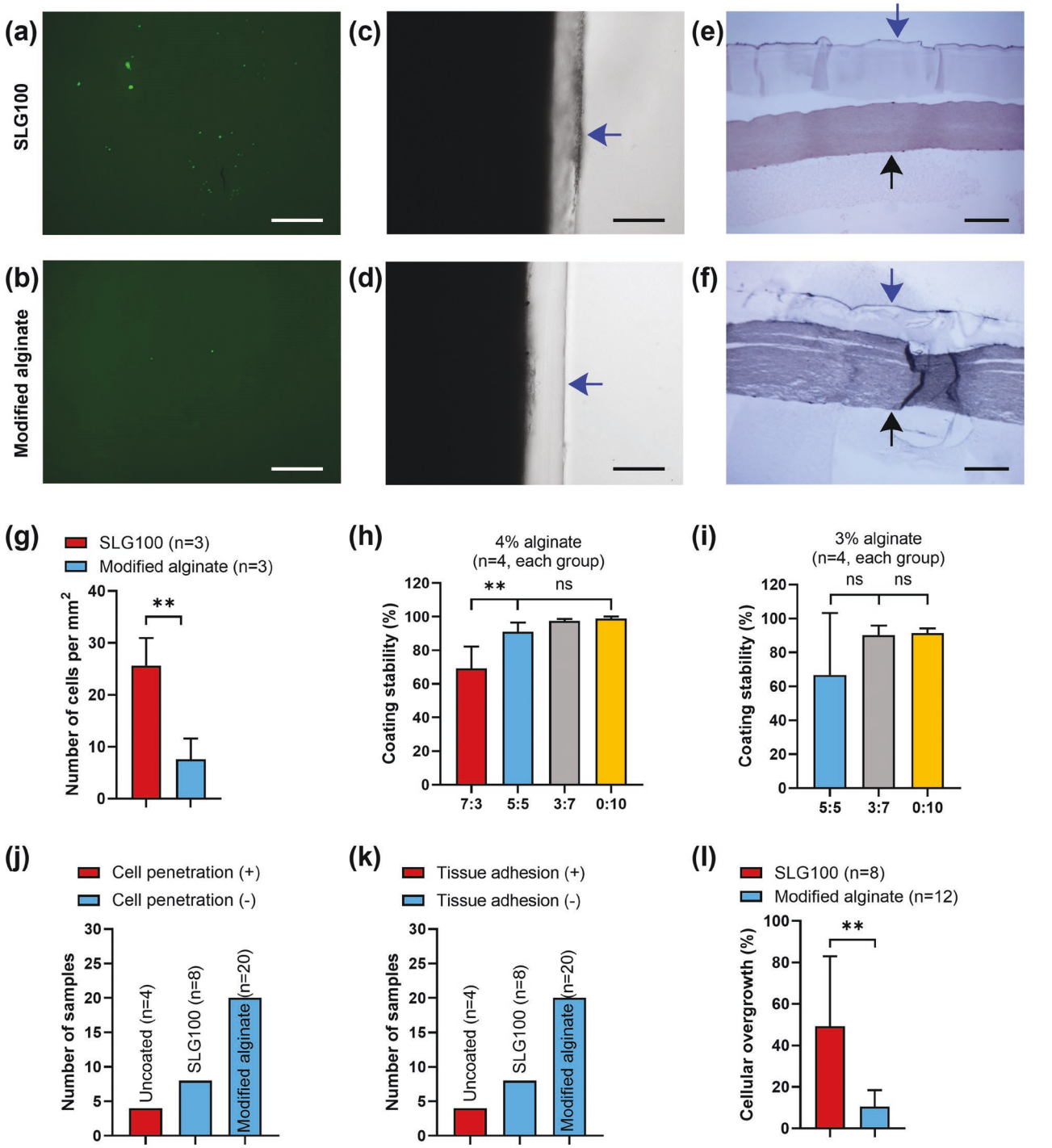

Figure 4. Stable zwitterionic alginate coating results in superior biocompatibility. a,b) Images of in vitro cell attachment test on alginate hydrogel coating surface using NIH3T3/GFP cells, scale bars, 1 mm. c–f) Representative images of devices coated with alginate hydrogels after 14-day in vivo test in the intraperitoneal space of healthy C57BL6/J mice; blue arrows point to the outer surface of coated devices, while black arrows point to the nanofiber membranes (the black areas in (c),(d) are also nanofiber membranes), the scattered dots on the alginate surface in (c–f) are attached cells, scale bars, 200 µm. a,c,e) 3% SLG100. b,d,f) 3% modified alginate (SB-alginate:SLG100 = 3:7). g) Quantification of the cell attachment on the device after 1 day incubation. h,i) Quantification of coating stability for alginate hydrogels with different ratios between SB-alginate and unmodified high molecular weight alginate SLG100 (n = 4 for each ratio, combinations of devices retrieved on day 14 and day 28, 0:10 represents neat SLG100): h) 4% alginate; i) 3% alginate. j,k) Number of samples having j) cell penetration and k) tissue adhesion for uncoated devices, devices coated with neat SLG100 and modified alginate. Neat SLG100 (n = 8) is a combination of samples from concentration of 3% and 4%, while modified alginate (n = 20) is a combination of samples from 3% modified alginate (3:7 & 5:5) and 4% modified alginate (3:7, 5:5 & 7:3). l) Quantification of cellular overgrowth on coated devices. Neat SLG100 (n = 8) is a combination of samples from concentration of 3% and 4%, while modified alginate (n = 12) is a combination of samples from 3% (3:7) and 4% (3:7 & 5:5).

4 weeks, devices were imaged immediately after retrieval and then processed with histological sectioning and H&E staining (Figure 4c–f). At a total alginate concentration of 4%, the coating was relatively unstable when the ratio was 7:3, with ≈69% coated hydrogel remaining on the device after retrieval based on H&E images. However, the other two ratios (5:5, 3:7) had >90% coated hydrogel remaining, which was comparable to that of neat SLG100 (i.e., 0:10) coating (Figure 4h and Figure S8, Supporting Information). Since a lower concentration is expected to provide better mass transfer, we further tested 3% alginate concentration with 5:5, 3:7, and 0:10 ratios. While the 5:5 ratio resulted in relatively unstable coating with a large variation (≈67% coated hydrogel remaining), the 3:7 and 0:10 ratios led to much more robust coatings (≈90% coated hydrogel remaining, Figure 4i and Figure S9, Supporting Information).

Notably, even with some hydrogel detachments (5:5 at 3% and 7:3 at 4%), cell penetration was not observed in the detached areas, likely due to the formation of hydrogel within the interconnected pores (Figure 4j, Figures S8c and S9c, Supporting Information), suggesting that the coating and the nanofiber membrane together provided synergistic protections. In addition, tissue adhesion was not observed for any coated devices (20 for modified alginate coating and 8 for neat SLG100 coating), including those having alginate detachment, suggesting the excellent biocompatibility of SB-alginate hydrogels (Figure 4k). More importantly, the modified alginate coatings (both 3:7 at 3% and 5:5, 3:7 at 4%) exhibited significantly less cellular overgrowth than the neat SLG 100 (Figure 4c–f,l, Figures S8 and S9, Supporting Information), consistent with the results we observed for alginate microcapsules.[18] In general, the hydrogel coating with either neat SLG100 or modified alginate prevented the devices from being fully covered by cellular overgrowth. Additionally, the cellular overgrowth was usually thin, with only one or two layers of cells. In contrast, uncoated devices were usually entirely covered by a layer of cellular overgrowth with varying thickness (Figure S4k–o, Supporting Information). It should be noted that thick cellular overgrowth with a complete coverage should be avoided to enable the long-term function of encapsulated cells. To be quantitative, the cellular overgrowth on coated devices was characterized by the percentage of cell coverage according to H&E histology images from entire devices. In particular, the devices coated with modified alginate hydrogels had a much smaller percentage of cellular coverage relative to those coated with neat SLG100 when comparing corresponding concentration of 3% or 4% (Figure S9j,k, Supporting Information). In addition, no significant difference was detected between 3% and 4% for both neat SLG100 and modified alginate (Figure S9l,m, Supporting Information). The reason for the reduced fibrosis of modified alginate may be attributed to the superior antifouling properties due to the strong hydration of the SB groups, which can prevent non-specific protein adsorption and inhibit inflammatory reactions.[18]

2.5. SHIELD Supports Long-Term Function of Rat Islets in C57BL6/J Mice

To evaluate the efficacy of SHIELD, we encapsulated rat islets (600 islet equivalents (IEQs)) and transplanted them in the intraperitoneal space of streptozotocin (STZ) induced C57BL6/J diabetic mice. Devices coated with 3% (n = 4) and 4% (n = 11) modified alginate both at 3:7 ratio were investigated; devices coated with 3% neat SLG100 (n = 4) and uncoated devices (n = 3) were included as controls. According to the blood glucose data, the devices coated with modified alginate showed much better performance than those coated with neat SLG100 or uncoated devices (**Figure 5**a). Although all mice treated with devices became normoglycemic shortly after transplantation (20 mice in 2 days, 1 mouse in 4 days), mice treated with uncoated devices maintained a short period of normoglycemia and all returned to the diabetic state within 12 days. In contrast, normoglycemia was greatly extended when devices were coated with alginate. Notably, three out of four devices coated with 3% modified alginate and nine out of ten devices coated with 4% modified alginate (1 false-diabetic mouse was excluded) were able to control the blood glucose for >100 days, while the 100-day cure rate for 3% neat SLG100 coating was only one out of four. With modified alginate coating, seven SHIELDs were still functional when retrieved for up to 399 days (detailed information about all mice is summarized in Table S1, Supporting Information). During the cure time, the rate of high blood glucose (≥210 mg mL^{-1}) for both 3% and 4% modified alginate coating was much lower than that of 3% neat SLG100 coating, indicating better control of blood glucose from SHIELDs (Figure S10a,b, Supporting Information). Importantly, the body weight increase (after ≈50 days implantation) of both 3% and 4% modified alginate coated device group was significantly higher than that of 3% neat SLG100 coated device group (≈22%) (Figure S10a,c, Supporting Information), indicating better performance for modified alginate coating.

To verify the function of implanted devices, oral glucose tolerance tests (OGTT) were performed at various time points (day 50 for mice receiving uncoated devices, day 273 for those receiving devices coated with 3% modified alginate, and day 192, 342, 398 for those receiving devices coated with 4% modified alginate). Similar glucose clearance profiles were observed between the modified alginate coated device group and the healthy control group. In contrast, only a slight blood glucose decrease was observed for the mice treated with uncoated devices (Figure 5b). Importantly, all devices coated with modified alginate (n = 15) and neat SLG100 were found without any tissue adhesion during retrieval (Movie S4), while 2 out of 3 uncoated devices had tissue adhesion (Figure S10d, Supporting Information). After retrieval of engrafted SHIELDs, blood glucose increases and body weight decreases (≈1.4 g in ≈2 weeks) were generally observed, confirming that the normoglycemia was attributed to the therapeutic function of the implanted devices (Figure 5a and Figure S10a,e, Supporting Information). Furthermore, ex vivo Glucose-stimulated insulin secretion (GSIS) was performed for the retrieved devices. Moderate insulin secretion was detected, indicating the maintained function of encapsulated islets in the devices after long-term implantation (Figure S10f, Supporting Information). Imaging of islets harvested from retrieved devices indicated that most islets remained healthy with a round shape and rare necrosis (Figure 5e). The H&E images and insulin/glucagon staining also confirmed the intact islet morphology and function (Figure 5f,g).

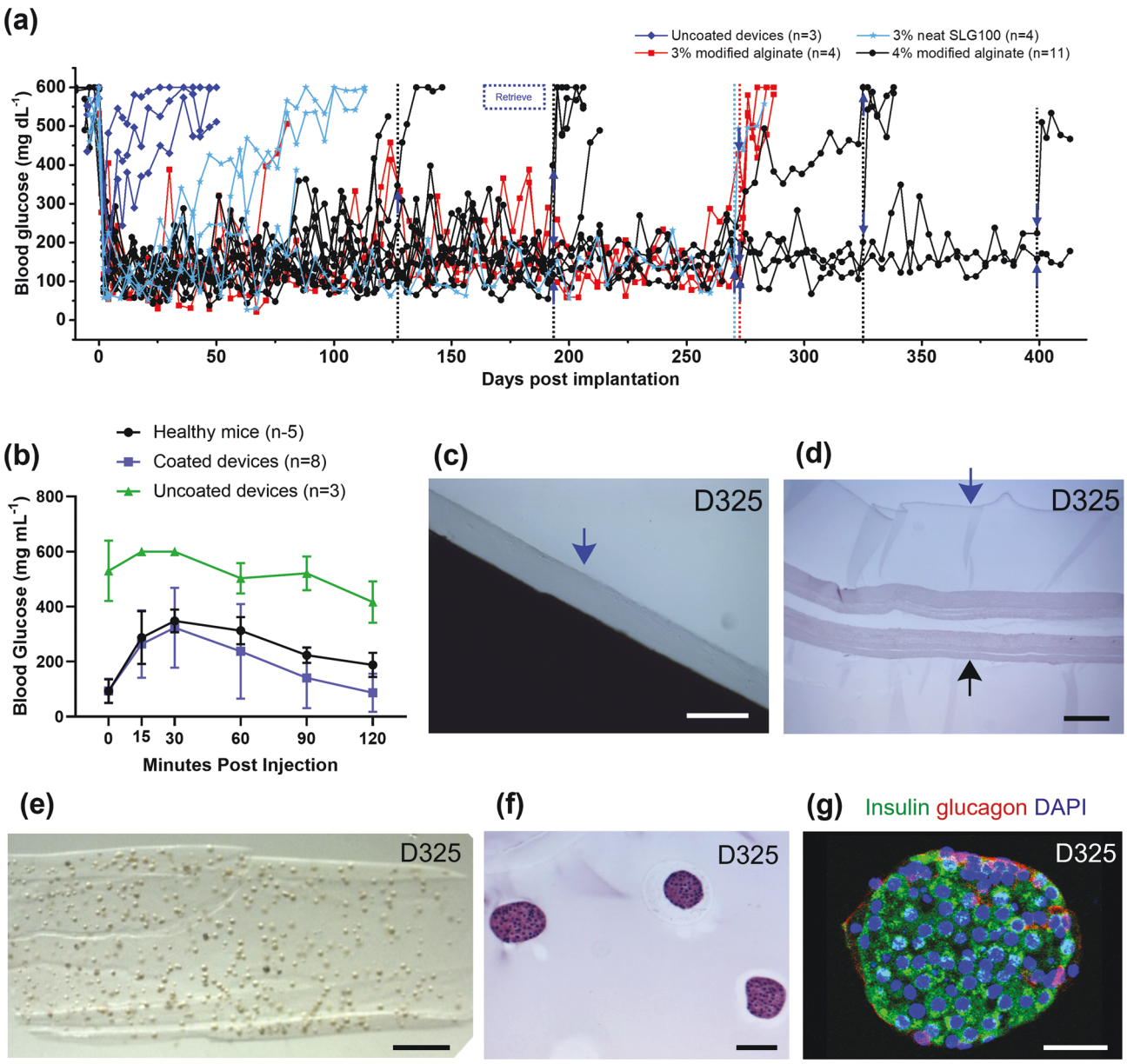

Figure 5. SHIELD supports long-term function of rat islets in C57BL6/J mice. a) Blood glucose as a function of days post implantation (retrieval is indicated by blue arrows together with colored dash lines corresponding to blood glucose curves). b) OGTT for healthy mice ($n = 5$), diabetic mice treated with modified alginate coated devices (a combination of all modified alginate coated devices longer than 193 days, $n = 8$) and uncoated devices (on day 50, $n = 3$). c,d) Images of a SHIELD device retrieved on day 325 showing rare cellular overgrowth, blue arrows point to the outer surface, while black arrows point to the nanofiber membrane (the black area in (c) is also nanofiber membrane), scale bars, 200 µm c) an optical image d) an H&E image. e–g) Images of islets in a SHIELD retrieved on day 325: e) an optical image, scale bar, 10 mm; f) an H&E image, scale bar, 100 µm; g) insulin/glucagon/DAPI staining, scale bar, 25 µm.

We next further evaluated the coating stability and cellular overgrowth of the retrieved devices. Compared to short-term (2–4 weeks) studies, coating stability of 3% modified alginate (3:7) seemed to decline slightly after long-term studies (82 days ($n = 1$) and 274 days ($n = 3$)), but it was not statistically significant (Figure S10g, Supporting Information). In contrast, both 3% neat SLG100 and 4% modified alginate hydrogel coating exhibited a good long-term stability, significantly better than 3% modified alginate hydrogel coating (Figure S10h, Supporting Information). In general, the function of islet encapsulation devices was highly dependent on cellular overgrowth. For example, up to 80% coverage of cellular overgrowth was observed on devices that had failed before retrieval (Figure S10i,l, Supporting Information). In contrast, most functional devices had minimal cellular overgrowth (≈10% coverage) (Figure 5c,d, and Figure S10i, Supporting Information). However, elevated cellular overgrowth was observed from 3% modified alginate coating (Figure S10j, Supporting Information), which could be

induced by the coating defects generated during long-term in vivo test due to less coating stability. In addition, the longer time of in vivo test might also contribute to more fibrosis. Statistically, long-term implantation with islets resulted in increased cellular overgrowth (≈38% coverage) compared to that of short-term without islets (≈11% coverage) (Figure S10k, Supporting Information). Encouragingly, the cellular overgrowth for 4% modified alginate coating was much less than that of 3% neat SLG100, indicating that modified alginate indeed performed better in resisting fibrosis (Figure S10j, Supporting Information). Furthermore, the varied fibrosis and function for the same coating conditions could be attributed to the individual difference of immune systems among different mice.

2.6. SHIELD Supports Long-Term Function of Human SC-β Cells in SCID-Beige Mice

The most impactful application of a safe, scalable, and long-term functional encapsulation device is to deliver human SC-β cells. To test the feasibility, we encapsulated human SC-β cells and transplanted them into STZ-induced immunodeficient SCID-Beige diabetic mice. Uniform clusters (≈150 µm) of SC-β cells were prepared by aggregation of single cells (Figure S11a, Supporting Information), and 3% modified alginate (3:7) was used for the device coating after preliminarily confirming the blood glucose results of rat islet encapsulation. Each mouse was transplanted with a device encapsulating ≈4500 clusters. Most devices (13 out of 15) corrected diabetes shortly (within 2–5 days) after implantation and remained functional for up to 238 days (**Figure 6**a). Among the functional devices, only one failed within 100 days, and three failed between 100 and 200 days (detailed information about all mice is summarized in Table S2, Supporting Information). At ≈50 days after implantation, body weight increased by ≈22%, significantly higher than that of the diabetic control group (Figure S12a,b, Supporting Information). OGTT tests revealed that the treated mice exhibited significantly better glucose clearance than untreated diabetic controls, confirming the function of encapsulated SC-β cells (Figure 6b).

Human C-peptide was quantified by measuring the concentration in mouse serum using an ELISA kit. Results confirmed that implanted SC-β cells secreted human C-peptide in all treated mice for both short-term and long-term studies (Figure S12c, Supporting Information). Although the amount of C-peptide seemed to decrease over time, the fact the human C-peptide was detected after 234 days of implantation indicated the potential of this device for SC-β cell encapsulation. To further verify the function of implanted devices, mice were kept alive after retrieving the devices. Importantly, blood glucose increased and body weight decreased for all mice after device retrieval (Figure 6a and Figure S12d, Supporting Information), confirming that the restoration of normoglycemia was due to the implanted devices. We attributed the success of the devices to the stability and superior biocompatibility of the modified alginate coating. Overall, all devices (n = 15) were free of tissue adhesion, and 3% modified alginate coating for most devices (13 out of 15) remained stable. However, 4% modified alginate coating might be used to provide more reliable protection (Figure S12e, Supporting Information). Despite a high density of encapsulated human SC-β cells, cellular overgrowth on most devices (14 out of 15) in SCID-beige mice was as mild as observed during short-term implantation in C57BL6/J mice (Figure 6c,d, and Figure S12f, Supporting Information). Most cell clusters in retrieved devices were healthy and functional, containing C-peptide/insulin-positive cells with PDX1 expression as well as glucagon-positive cells (Figure 6e–g and Figure S11b–d, Supporting Information).

2.7. Scalability and Retrievability of SHIELD in Dogs

The scalability of an encapsulation device is required for clinical applications.[22] Enabled by our unique design, SHIELD can be scaled up in both radial and longitudinal directions without affecting the diffusion distance. If the islet density of 4500 IEQs per 80 µL is used, a 3.1-m-long device (inner tube diameter: 2 mm) will be needed to achieve a therapeutic dosage of 700 000 IEQs for a typical 70 kg T1D patient. However, if the inner tube diameter is increased to 20 mm, the length needed would be around 38.5 cm. As a proof-of-concept for scalability and retrievability, long devices (length ≈12 cm, ID 3.2 mm) were fabricated and intraperitoneally implanted into healthy dogs (n = 3). Considering the occasional coating detachment for 3% modified alginate (3:7), 4% modified alginate (3:7) was used for the dog experiment. Uniform coating along the entire length of the device was achieved using the "in-out crosslinking" method (**Figure 7**a). To prevent kinking which may happen for long devices, a nylon ribbon was inserted into the inner lumen to ensure a stable shape while maintaining flexibility. The nylon ribbon was around 0.5 mm thin and 3 mm in width. By inserting the nylon ribbon, the inner nanofibrous tube became relatively flat rather than circular or oval, preventing SHIELD from compression from any direction. In addition, the lumen of the inner nanofibrous tube was almost occupied by the nylon ribbon, which can save the peritoneal space needed, especially after scaling up SHIELD in the radial direction. Notably, SHIELD was still flexible along the length direction, making it adaptable to the complex geometry of peritoneal space in dogs. Finally, the slender geometry allowed us to implant the device using a minimally invasive laparoscopic procedure. Among the three dogs, one was implanted with the device without any anchoring. In the other two dogs, the devices were anchored to the body wall through a nylon suture for rapid localization and convenient retrieval (Figure 7c–f and Movie S5, Supporting Information). The suture was bonded to one end of the device by thermo sealing and coated with PDMS to mitigate tissue adhesion (Figure 7b). In addition, the suture extended ≈10 cm away from the peritoneal wall to provide freedom for the device movement and minimize irritation to surrounding tissues (Figure 7f and Movie S6, Supporting Information).

Devices were retrieved after 1 month using a similar laparoscopic procedure. No adhesion to any organs occurred for all three devices except mild adhesion to omentum which could be easily separated by electrocautery and retrieved laparoscopically (Figure 7g–i, Figures S13a,S14, Supporting Information, Movies S7 and S8, Supporting Information), suggesting that SHIELD was safe and retrievable. Notably, for one of the suture-anchored devices, omentum adhesion only occurred to

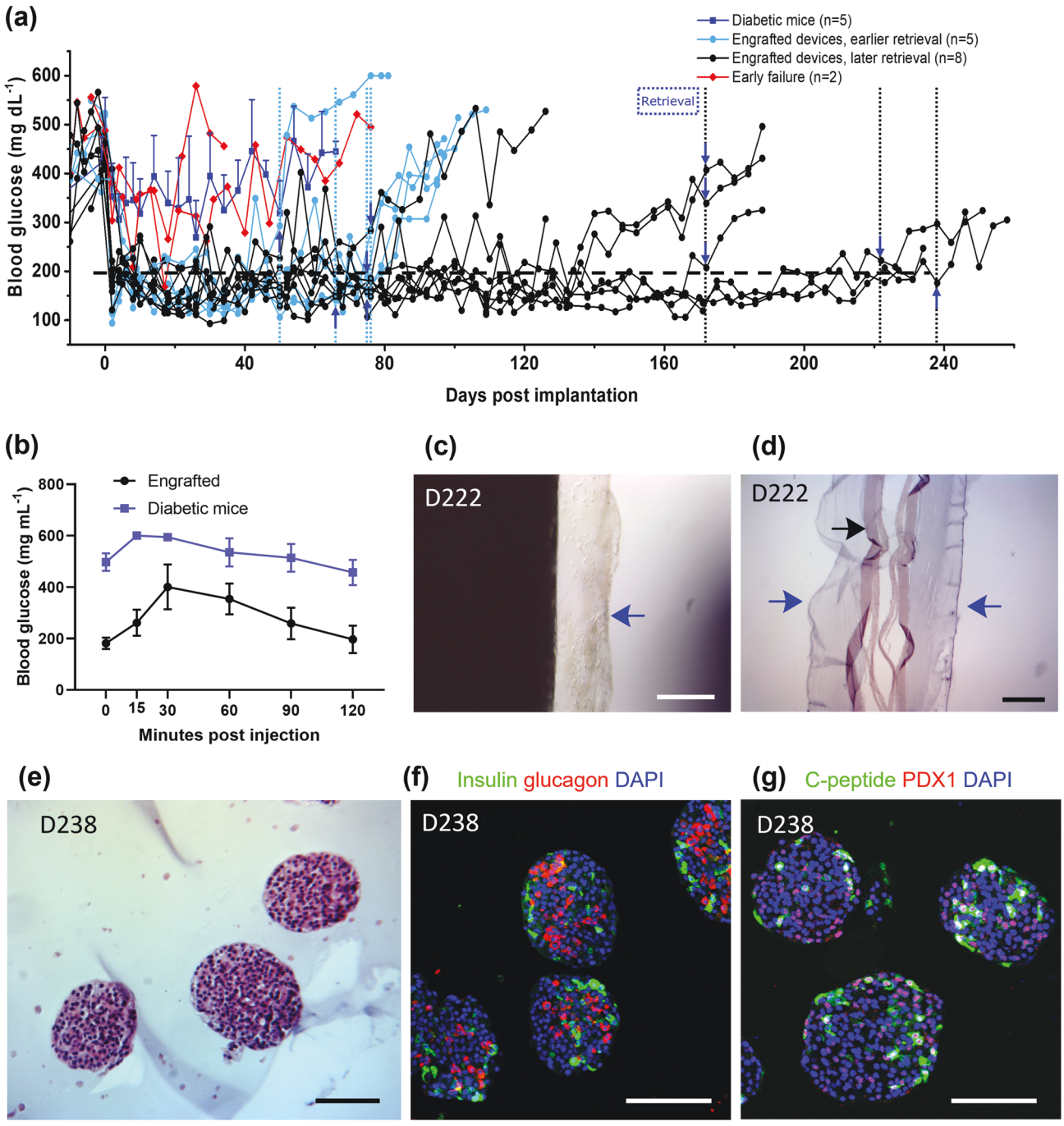

Figure 6. SHIELD supports long-term function of human SC-β cells in SCID-beige mice. a) Blood glucose as a function of days post implantation (retrieval is indicated by blue arrows together with colored dash lines corresponding to blood glucose curves). b) OGTT for diabetic mice ($n = 4$) and mice having engrafted devices (day 45 and day 61, $n = 9$). c,d) Images of a SHIELD retrieved on day 222 showing mild cellular overgrowth, blue arrows point to the outer surface, while black arrows point to the nanofiber membrane (the black area in c is also nanofiber membrane), the scattered dots on the alginate surface are attached cells, scale bars, 200 µm c) an optical image d) an H&E image. e–g) Images of islets in a SHIELD retrieved on day 238, scale bars, 100 µm: e) an H&E image; f) insulin/glucagon/DAPI staining; g) C-peptide/PDX1/DAPI staining.

one end near the anchoring point while the rest was free of adhesion (Figure 7g–i, Figure S13a, Supporting Information), indicating the excellent performance of the modified alginate coating. Optical images and H&E staining indicated that most of the device was still covered with alginate hydrogels (Figure 7j–l, Figure S13b–f, Supporting Information). Except for the adhesion end (Figure 7m, Figure S13b, Supporting Information), cellular overgrowth was minimal and comparable to the device in mice (Figure 7k,l, Figure S13c–f, Supporting Information), underscoring the excellent biocompatibility of modified

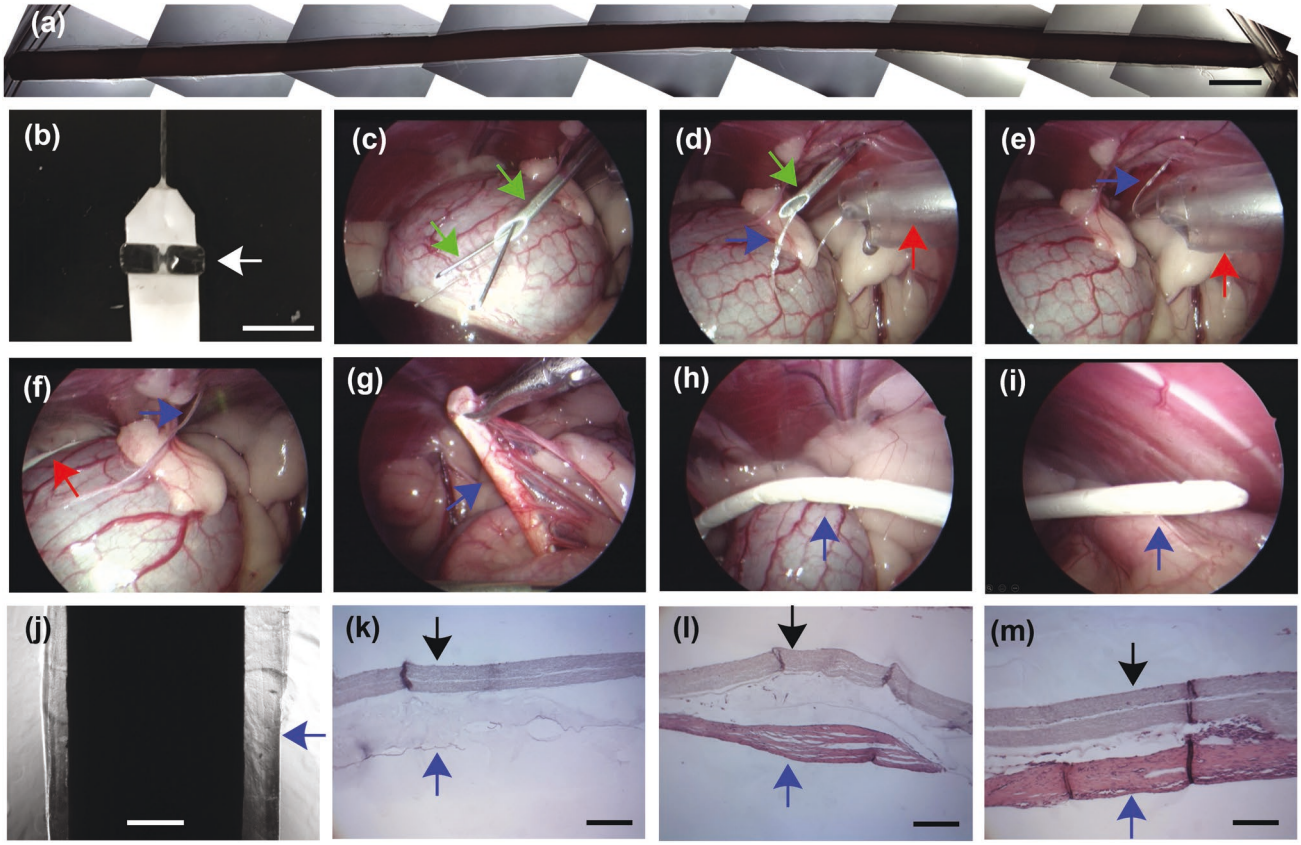

Figure 7. Scalability and retrievability of SHIELD in dogs. a) A hanging-suture SHIELD before implantation (4%, 3:7 modified alginate coating, length ≈ 12 cm), scale bar, 5 mm. b) An image showing one end of a hanging-suture SHIELD was bonded to a nylon suture with the arrow pointing to translucent thermo bonded area, scale bar, 5 mm. c–e) Images showing the anchoring process using a suture grasper; green arrows point to the suture grasper, blue arrows point to the hanging suture connecting the SHIELD, and red arrows point to the SHIELD being delivered through a trocar, scale bars, 5 mm: c) open the grasper; d) catch the hanging suture; e) withdraw the grasper together with the hanging suture. f) An image showing a device free in the abdomen with the suture passing through the peritoneal layer of the body wall. g–i) Images showing a device after 1-month implantation: g) adhesion to omentum occurred on one end; h,i) the majority of the device was free of adhesion as shown by blue arrows. j–l) Images showing minimal cellular overgrowth on the surface of coated alginate hydrogel; blue arrows point to the outer surface, while black arrows point to the nanofiber membrane (the black area in j is also nanofiber membrane): j) an optical image, scale bar, 1 mm; k,l) H&E images, scale bar, 200 µm. m) An image showing the cellular overgrowth in the area having omentum adhesion; blue arrows point to the cellular overgrowth, while black arrows point to the nanofiber membrane, scale bar, 200 µm.

alginate hydrogels. According to the H&E staining images (Figure S13b, Supporting Information), the omentum adhesion was likely induced by the coating defects at the sealing end. If the omentum adhesion could be avoided, the clinical use of cell encapsulation devices would be more acceptable. Nevertheless, our results suggest that the device can be scaled up, implanted, and retrieved using minimally invasive procedures.

3. Discussion

Cell encapsulation has the potential to provide a treatment free of compliance and immunosuppression for T1D. However, developing a device that simultaneously meets the requirements of safety, scalability, and long-term functionality is a great challenge. One of the major hurdles is the foreign body response against the encapsulation material. Cellular overgrowth and fibrotic deposition diminish the transfer of oxygen and nutrients to the cells, and insulin and metabolic wastes from the cells. Recent clinical trials using the ViaCyte device and the Beta-Air device have convincingly shown the foreign body response as a critical barrier for function.[14,17,18] Alginate hydrogels, either microcapsules or fibers, have shown promising biocompatibility in animal studies. Further chemical modifications can drastically improve its biocompatibility, significantly reducing the foreign body response-induced cellular overgrowth and fibrosis. However, hydrogels are intrinsically weak and easy to swell or break, posing a safety concern for clinical applications, especially when SC-β cells are transplanted.

Here we report SHIELD, a novel device which combines the safety of a retrievable device and the biocompatibility of zwitterionically modified alginate. Several innovative design features, which enable translation, are worth reiterating. First, the device has a concentric configuration with cells encapsulated in the cylindrical wall. Compared with previously reported tubular or fiber devices,[22,28] SHIELD allows scale-up not only in the longitudinal but also radial directions without significantly sacrificing diffusion distance and thus mass transfer. In principle,

a clinically relevant cell loading capacity may be achievable with a reasonable length (i.e., on the order of tens of centimeters instead of meters). Second, SHIELD employs an electrospun nanofibrous membrane as the primary barrier to prevent cell escape or penetration, bestowing ideal qualities for cell encapsulation, including excellent mechanical properties, high porosity, and tunable, interconnected pore structures. These properties enable optimization of mass transfer while ensuring safety that is of utmost importance for delivering SC-β cells in clinical applications. Third, enabled by our unique "in-out crosslinking" strategy, SHIELD features a thin, uniform, durable hydrogel coating of zwitterionically modified alginate, mitigating cellular overgrowth for long-term implantation. It should be noted that both the biocompatibility and quality of the hydrogel coating are important to achieve long-term function of this type of cell encapsulation devices.

We systematically investigated the pore size of the nanofibrous membrane and coating conditions to achieve SHIELD with balanced safety and functionality. We showed that the optimized SHIELD significantly reduced cellular growth compared to uncoated devices or those coated with neat SLG100. As a result, we demonstrated that the device could support long-term function of rat islets in immunocompetent mice for up to 399 days. More importantly, we found human SC-β cells at a high density survived in the device and restored normoglycemia of immunodeficient diabetic mice shortly after implantation without any maturation period, for up to 238 days. Lastly, large-animal studies demonstrated SHIELD's scalability and retrievability by intraperitoneal implantation of 12 cm-long devices in dogs. The devices could be conveniently implanted and rapidly retrieved using minimally invasive laparoscopic procedures. All these results provide a proof of concept for the potential of SHIELD to safely deliver human SC-β cells to T1D patients.

Challenges remain for SHIELD to realize its full potential. While most devices protected encapsulated cells and maintained normoglycemia for a long-term, some failed after 100 days. Post-retrieval analysis indicated that the failure or compromised function was likely caused by relatively severe cellular overgrowth, resulting in declined mass transfer. Therefore, further research and development of fibrosis-mitigating materials is highly desired. Nevertheless, our unique device design enabled high graft rate and long cure time for both rat islets and SC-β cells in mice, which are inspiring for scaled SHIELD. These results are particularly attributed to the development of the "in-out crosslinking" strategy that enabled robust and controllable alginate coating to overcome the intrinsic weak mechanical properties of alginate hydrogels. SHIELD represents a significant progress toward the goal of developing cell encapsulation devices which mitigate or eliminate foreign body responses in large animals and ultimately humans, while also providing safety, scalability, and retrievability; such devices may benefit the entire field of cell encapsulation, both for T1D and other hormone deficiency diseases.

4. Experimental Section

Materials: Poly (caprolactam) (nylon 6, 181 110), formic acid (FA, F0507), thrombin from bovine plasma (T4648), fibrinogen from bovine plasma (F8630), streptozotocin (STZ, S0130) and gelatin from porcine skin (G1890) were purchased from Sigma-Aldrich Co. (St. Louis, MO). 1,1,1,3,3,3-Hexafluoro-2-propanol (HFIP, 0 03409) was purchased from Oakwood Products, Inc. (Estill, SC). Calcium chloride ($CaCl_2$, BDH9224) and sodium chloride (NaCl, BDH9286) were purchased from VWR International (Radnor, PA). Barium chloride dihydrate ($BaCl_2.2H_2O$, BX0060-1) was purchased from EMD Millipore Corporation. Regular sodium alginate (PROTANAL LF 10/60FT) and sterile sodium alginate (Pronova SLG 100) were purchased from FMC BioPolymer Co. (Philadelphia, PA). Sucrose (8360-6) was purchased from Avantor Performance Materials, LLC. (Center Valley, PA). All reagents were used without further purification. Sulfobetaine-modified alginate (SB-alginate) was synthesized according to a previously published protocol.[18]

Animals: C57BL/6J mice were purchased from Jackson Lab. SCID-beige mice were purchased from Taconic Farms. Sprague-Dawley rats were purchased from Charles River Laboratories. Beagle dogs were purchased from Marshall Bioresources. All animal procedures were approved by the Cornell Institutional Animal Care and Use Committee (Protocol number: 2012-0144).

Electrospinning: Nanofiber tubes were fabricated by electrospinning of nylon 6 (PA6) solutions. To fabricate nanofiber tubes with controllable fiber diameter, pore size, thickness, and good uniformity, a customized electrospinning setup was developed for SHIELD (Figure S4a, Supporting Information). In particular, uniformity was achieved by using a rotating collector and a moving stage. Both speeds were precisely regulated by a controller. Specifically, the moving stage enables the back-and-forth movement of the spinning nozzle and thus the uniform deposition of nanofibers on the collector that rotates simultaneously. Importantly, both the travel length of the moving stage and the length of the collector can be adjusted with ease to fabricate tubes with different lengths. Unless otherwise noted, the diameter of rod collectors, collecting distance, rotating speed of collecting rod, and the speed of moving stage were kept constant at 3.2 mm, 8 cm, 375 rpm, 3.48 m min^{-1}, respectively. Detailed electrospinning parameters for different pore sizes can be found in Table S3, Supporting Information. It should be noted nanofiber membranes with an average pore size of 1.05 µm were used for most studies unless otherwise noted.

To achieve good reproducibility, not only a highly controllable electrospinning setup is needed, but also stable recipes for the polymer solutions and electrospinning. By using hexafluoroisopropanol (HFIP) and HFIP/FA (8/2, v/v) solvent systems, stable electrospinning of nylon 6 (PA6) solutions was achieved without needle clog, making it possible to fabricate nanofiber tubes with reproducible and controllable quality. As a demonstration, >20 cm long nanofiber tubes were fabricated (Figure S4b, Supporting Information). Nanofiber tubes with different diameters were generated using conductive collecting rods with desired diameters (Figure S4c, Supporting Information). In addition, the thickness of nanofiber tubes was controlled by electrospinning time (Figure S4d, Supporting Information). While the average pore size was tailored by adjusting the diameter of nanofibers (Figure 2a and Figure S4f–j, Supporting Information). Furthermore, minimal influence of thickness on the pore size of nanofiber membrane was observed (Figure S4e, Supporting Information). Notably, the pore size has a significant influence in preventing cell penetration (Figure S4k–o, Supporting Information). While nylon 6 was used for this study, other polymers (polyurethane, polysulfone, polyacrylonitrile, polyethylene terephthalate, polyvinylidene difluoride, polyacrylamide, poly(ethyl methacrylate), poly(methyl methacrylate), polyvinyl chloride, polyoxymethylene, etc) compatible with electrospinning are also suitable for the fabrication of SHIELD.

To facilitate the removal of nanofiber tubes from rod collectors, a thin layer of sucrose syrup (25 g mL^{-1}) was coated on the rod collectors before electrospinning. After electrospinning, nanofiber tubes were removed and released from rod collectors by soaking in DI water. The sucrose was removed by washing with large volume DI water three times (at least 10 min each time). Then nanofiber tubes were placed on a clean surface to dry out. To remove the residual solvents, dry tubes were heated in a vacuum oven (Temperature 60 °C, Pressure 27 in. Hg) for 24 h.

Preparation of Sucrose Syrup: The sucrose syrup was prepared by adding 45 g of sucrose into 18 mL DI water in 50 mL a falcon tube and resulted in a ≈47 mL mixture after dissolution. The mixture was placed in an oven (132 °C) with the cap closed. Shaking was needed every 10 min for three times to accelerate the dissolving process. Once all the sucrose was dissolved (indicated by a colorless solution), the solution was kept in the oven (80 °C) for ≈24 h after removing the cap. Finally, the solution became viscous (≈42 mL) and turned golden brown. Then it was removed from the oven. The solution was stored at room temperature. If precipitation occurred, the solution was heated in the oven (132 °C) for 30 min to dissolve the precipitated sucrose. A regular sucrose solution displayed a low viscosity similar to water. In contrast, the sucrose syrup was made highly viscous via our protocol so that the sucrose would stay adhered to collecting rods long enough for fabrication. A low viscosity solution would result in discontinuous droplets on collecting rods in a second due to surface tension that would influence the shape of nanofiber tubes and make it difficult to remove the nanofiber tubes.

In-Out Crosslinking of Alginate: Outer nanofiber tubes (ID 3.2 mm, pore size 1.05 µm, dry) were cut into ≈2.5 cm long, and one end was sealed using a custom-designed thermo cutter (Figure S1, Supporting Information). Then one-end sealed nanofiber tubes were treated with 20% sodium hydroxide overnight to make them hydrophilic and facilitate the penetration of alginate precursor during in-out crosslinking. After washing away excessive sodium hydroxide, nanofiber tubes were sterilized by autoclave (120 °C, 20 min). Unless otherwise noted, the length, diameter, and average pore size of nanofiber tubes were kept constant at 2.5 cm, 3.2 mm, 1.05 µm, respectively.

During in-out crosslinking, a stainless-steel capillary (OD ≈ 2.5 mm) connected to a syringe (filled with crosslinking buffer, 200 mM $BaCl_2$) was inserted into the one-end sealed nanofiber tube. The nanofiber tube was first dipped into coating alginate precursor, allowing the penetration of alginate precursor into the nanofiber membranes, thus forming alginate hydrogels after crosslinking in the interconnected pores of nanofiber membranes. Next, the nanofiber tube was filled with crosslinking buffer that diffused through the porous membranes of nanofiber tubes and crosslinked alginate. The diffusion time was controlled to achieve alginate hydrogel coating with a desired thickness. Then uncrosslinked alginate precursor was washed away immediately after a specific diffusion time by shaking the stainless capillary with the nanofiber tube in a reservoir filled with saline. Finally, these coated nanofiber tubes were further crosslinked (200 mM $BaCl_2$) and washed with saline at least six times to remove residual crosslinkers. It is important not to contaminate the dry nanofiber tubes with crosslinking buffer before soaking them in alginate solution. Otherwise, the penetration of alginate precursors will be prevented, resulting in poor coating adhesion between alginate hydrogels and nanofiber membranes.

Fabrication of SHIELD: Nanofiber tubes (OD 2.2 mm, pore size 1.67 µm, thickness 200 µm, dry) were cut into 2 cm long and sterilized by autoclave (120 °C, 20 min) to prepare inner nanofibrous tubes. Next, inner nanofibrous tubes were soaked in crosslinkers (5 mM $BaCl_2$ 95 mM $CaCl_2$) for 20 s. Meanwhile, cells were mixed with 2% SLG100. Then, excessive crosslinkers were removed using sterile napkins. It was crucial to make sure that no visible liquid was left in the lumen. Before applying 80 µL volume cells/SLG100 mixture, one arm of a tweezer was inserted into the lumen of an inner nanofibrous tube for rotating while applying cells/alginate precursor around it. Once uniform cell loading was achieved, inner nanofibrous tubes were further crosslinked in the crosslinking solution for 4 min. Then an inner nanofibrous tube was inserted into an outer nanofibrous tube (coated by in-out crosslinking method, ID 3.2 mm, pore size 1.05 µm, length ≈2.5 cm, thickness 140 µm) immediately followed by six times of washing. Finally, the open end of the outer nanofibrous tube was sealed with a custom-designed thermo cutter (Figure S1, Supporting Information). In addition, the sealing end was applied with coating alginate precursor and crosslinked in 200 mM $BaCl_2$ for 30 s. After washing six times, SHIELDs were imaged and incubated for at least 1 h before implantation. It should be noted that saline was the washing buffer and was also used for dissolving alginate for rat islets encapsulation. While saline was replaced with HBSS for encapsulation of human SC-β cells. We expected to use the thinnest possible outer nanofibrous tubes as the thickness determines the diffusion distance. From our investigation, 140 µm was the thinnest membrane that could maintain the tubular structure during alginate coating. Further decreasing the thickness resulted in insufficient mechanical stability. Therefore, 140 µm was chosen for the outer nanofibrous tubes. At the same time, 200 µm was selected for the inner nanofibrous tubes due to better mechanical properties to provide reliable structural support for the surrounding cells and hydrogels. In addition, the thickness of the inner nanofibrous tubes is not likely to influence the mass transfer.

The dosage of each device was controlled by dispersing 80 µL 2% SLG100/islets mixture around the inner nanofibrous tube 600 IEQs for rat islets or 4500 clusters for human SC-β cells). The existence of pre-loaded crosslinkers (95 $CaCl_2$, 5 mM $BaCl_2$ in saline) in the pores of inner nanofibrous tubes allowed for the uniform dispersion and in situ crosslinking of alginate/islets mixture in ≈1 min. By making full use of the shrinking (in crosslinkers) property of alginate hydrogels, a typical SHIELD was achieved by inserting a freshly crosslinked inner nanofibrous tube to a pre-coated outer nanofibrous tube. Post-insertion washing in saline and incubation in medium permitted the equilibration and swelling of alginate hydrogels, which rendered the well-fit SHIELD having islets distributed in the wall between the inner and outer nanofibrous tubes and thus ensured a short diffusion distance.

Characterizations of SHIELD: Nanofibers were imaged by a field emission scanning electron microscopy (Zeiss-Gemini-500-FESEM). The diameter of nanofibers was determined by analyzing the SEM images using Adobe Acrobat (Adobe, San Jose, CA). The pore size of the nanofiber membranes was measured using a capillary flow porometer (PMI, CFP-1100-AEHXL).

Mechanical Tests: Mechanical properties were measured using a mechanical testing machine (Instron 5965). Specifically, a tensile test (tensile rate 50 mm min^{-1}, clamping distance 20 mm) was conducted to determine the mechanical properties of nanofiber tubes (diameter 3.2 mm, thickness 140 µm, length 30 mm). For dip-coated samples, the fabrication procedure was quite close to the in-out crosslinking method, except for the timing of injecting the crosslinker. Specifically, the dip-coated samples (Figure 2c,d) were prepared by injecting crosslinkers first, to prevent the penetration of alginate precursors into nanofiber membranes. A peeling test was conducted to determine the coating fidelity (tensile rate 50 mm min^{-1}, clamping distance 20 mm, sample width 10 mm). The samples for the peeling test were prepared by in-out crosslinking with minor modifications. Particularly, only partial length (≈2 cm) of the devices was soaked in alginate precursor first to allow the alginate penetration. Then the nanofiber tubes were moved ≈2 cm deeper after injecting crosslinkers to have an area without interlocked interaction for clamping. In addition, the coated tubes were cut along the length direction, resulting in a film (width 10 mm) for the peeling test. It should be noted that 3% regular sodium alginate (PROTANAL LF 10/60FT) in saline was used for the tensile and peeling tests and measured directly after crosslinking.

In Vitro Tests: NIH3T3/GFP mouse fibroblasts were used for the test of cell escape and cell attachment. NIH3T3 mouse fibroblasts were used for viability test, Live/Dead staining was conducted according to the manufacturer's protocol (ThermoFisher) and imaged using an inverted fluorescent microscope (EVOS fl). All samples were cultured in DMEM supplemented with 10% FBS and 1% P/S. The medium was changed every other day. The culture environment was maintained in a 37 °C incubator with 5% humidified atmosphere of CO_2.

For the cell escape test, cells were dispersed in 20 mg mL^{-1} fibrinogen/saline and then mixed with 0.5 U mL^{-1} thrombin, 100 mg mL^{-1} gelatin/saline in a volume ratio of 1:1 to achieve a final concentration of 10 mg mL^{-1} fibrinogen, 0.25 U mL^{-1} thrombin, 50 mg mL^{-1} gelatin/saline solution with a cell density of 1 million mL^{-1}. Next, 60 µL cell-matrix suspension was filled into each one-end sealed, coated or uncoated nanofiber tube (length 2.5 cm, diameter 3 mm) using a 1 mL syringe connecting to a 23G blunt needle, followed by sealing using

a custom-designed thermo cutter (Figure S1, Supporting Information). Devices for the cell escape test were imaged on day 2, 5, 7, 10, and 14.

Presto blue assay was conducted on day 2, 3, and 4, respectively. Each sample was incubated with 400 µL 10% presto blue solution in a 500 µL Eppendorf tube for 1 h. After incubation, 100 µL incubated presto blue solution in triplicate was transferred to a 96 well plate for fluorescence reading. The excitation/emission wavelengths were 560/590 nm. The readings were normalized according to the background reading of 10% presto blue solution incubated without samples.

For the cell attachment test, coated nanofiber tubes were cut along the length direction into films. With the coated surface facing up and fixed by PDMS rings in six well plates, 3 mL cell suspension containing 2.5×10^6 NIH3T3/GFP cells were seeded on the coating surface. After 1 day incubation, each sample was gently transferred to a fresh medium and was imaged under an inverted fluorescent microscope (EVOS fl).

STZ-Induced Diabetic Mice: Male C57BL/6J mice purchased from Jackson Lab were intraperitoneally injected with 140 mg kg^{-1} STZ for diabetes induction. Successful diabetes induction was confirmed before implantation by at least two consecutive measurements of blood glucose > ≈500 mg dL^{-1}. Male SCID-beige mice purchased from Taconic Farms were intraperitoneally injected with 140 mg kg^{-1} STZ to induce diabetes. Successful diabetes induction was confirmed before implantation by at least two consecutive measurements of blood glucose > ≈350 mg dL^{-1}.

Islet Isolation: Sprague–Dawley rats obtained from Charles River Laboratories were used for islet isolation. First, the rats were anesthetized by 3% isoflurane in oxygen. Second, rat pancreases were cannulated with 0.16 mg mL^{-1} liberase (Roche Diagnostics GmbH) dissolved by M199 medium. Third, the pancreases were detached from other organs and collected into 50 mL falcon tubes (2 pancreases per tube) placed in an ice bath. Fourth, the pancreases were digested in 37 °C water bath for ≈30 min. The digestion was stopped by a cold RPMI medium supplemented with 10% FBS and 1% pen strep (purification medium). After vigorously shaking to break the pancreases into small pieces, twice more washing with purification medium was conducted. Then, pancreases were filtered by a 450 µm sieve. The supernatant was collected and rewashed with the purification medium. Next, cells were suspended in 20 mL Histopaque 1077 with 10 mL purification medium on the top and centrifuged at 1700 RCF (0 break and 0 acceleration) for 17 min at 4 °C (repeated twice). Furthermore, the islets were collected from the interface of Histopaque 1077 and purification medium. Islets were further purified by gravity sedimentations and handpicking to remove impurities. Finally, islets were washed once with purification medium and incubated overnight in a low adhesion petri dish with purification medium for further use.

Aggregation of Human SC-β Cells: Human SC-β cells were provided by Novo Nordisk. During the aggregation process, ≈2.2 million mL^{-1} single cells in re-aggregation medium were first seeded into a 250 mL flask (Corning, #431 144). The flask was placed on an orbital shaker (70 rpm) in a 37 °C incubator with 5% humidified atmosphere of CO_2. After 48 h, the re-aggregation medium was replaced with culturing medium and further cultured for 24 h. On day 3, the aggregated clusters were harvested for encapsulation.

Mouse Surgeries for Implantation and Device Retrieval: Mice were anesthetized using 3% isoflurane in oxygen. The ventral area was shaved and sterilized by betadine and 70% ethanol. A minimal incision with a length of ≈5 mm was made to implant the devices and was subsequently closed by a suturing process. Retrieval was conducted at different time points. If the blood glucose was under control, a survival procedure was conducted. The retrieval procedure was similar to the implantation except for a slightly longer (≈6–7 mm) incision length. It should be noted that the encapsulation device could be easily found by squeezing the device to the area where the incision was made. After retrieval, blood glucose was then further monitored to confirm that mice returned diabetic and previous normoglycemia was resulted from implanted devices. If the mice were hyperglycemic at the endpoint, devices in most mice were retrieved after euthanizing the mice.

Mouse Monitoring and Characterization: Blood glucose and body weight were measured every other day in the first week after implantation and twice per week afterwards. Blood was collected from the tail using a 27 G needle to prick the tail vein and analyzed using a Bayer Contour Next EZ blood glucose meter.

Oral glucose tolerance tests (OGTT) were conducted to assess the functionality of the devices. Specifically, mice were fasted for ≈12 h before injecting 2 g kg^{-1} D-glucose per body weight dissolved in tap water at a concentration of 320 mg mL^{-1}. Then blood glucose was measured at 0, 15, 30, 60, 90, 120 min.

When human SC-β cells were encapsulated and transplanted, human C-peptide was quantified by measuring mouse serum from non-fasting mice using ultra-sensitive ELISA kits (Mercodia) according to the supplier's protocol. About 200 µL facial vein blood was collected and clotted naturally for ≈15 min at room temperature. Then the clot was removed by centrifuging at 2000 rpm for 10 min, which resulted in ≈100 µL supernatant of serum.

Characterizations of Retrieved Devices: Retrieved devices were imaged under an optical microscope (EVOS fl) or stereomicroscope (Olympus SZ61) immediately after retrieval. Static GSIS was conducted for the retrieved devices using the Krebs Ringer Bicarbonate (KRB) buffer (135 mM NaCl, 3.6 mM KCl, 5 mM $NaHCO_3$, 0.5 mM NaH_2PO_4, 0.5 mM $MgCl_2$, 1.5 mM $CaCl_2$, 10 mM HEPES, 0.1% BSA) supplemented with 2 or 20 mM D-glucose. Specifically, each retrieved device was incubated in 2 mM D-glucose KRB buffer for 1 h to equilibrate, then sequentially incubated (1 h) in 2 and 20 mM D-glucose KRB buffers. It should be noted that 3 mL buffer was used for the GSIS test. The buffers at 2 and 20 mM D-glucose were collected for characterization using rat ultrasensitive insulin ELISA (ALPCO 80-INSRTU-E01, E10) according to the supplier's protocol.

Devices were fixed in 10% neutral buffered formalin and kept in 70% ethanol before being sent for histology. The retrieved devices were embedded in paraffin, sectioned (thickness 10 µm), and stained with H&E or Masson's Trichrome by Cornell Histology Core Facility. The H&E and Masson's Trichrome samples were imaged by a microscope (IN200TC, Amscope). The coating stability was qualified by dividing the area of the remaining coated alginate hydrogel after retrieval (according to H&E images) by that of the original alginate hydrogel coating. To be quantitative, the cellular overgrowth was characterized by two methods. For uncoated devices, thick cellular overgrowth with a complete coverage was usually found and therefore quantified by measuring the thickness of the fibrotic layer. In contrast, the cellular overgrowth on coated devices was very mild and usually not fully covered by cells, and therefore, it was characterized by the percentage of cell coverage. It should be noted that all the quantification was conducted according to H&E histology images from entire devices.

In addition, rat islets were further stained with insulin/glucagon/DAPI. Human SC-β cells were stained with C-peptide/PDX1/DAPI and insulin/glucagon/DAPI. Imaging was conducted by a laser scanning confocal microscope (LSM 710). To conduct immunofluorescent staining, the histological slides were deparaffinized, followed by antigen retrieval as described before.[29] Non-specific binding was blocked via incubation with 5% donkey serum (S30-M, Sigma) in PBS for 1 h at room temperature. Sections were then incubated with primary antibodies overnight at 4 °C. The sections were washed with PBS and incubated with the fluorescently conjugated secondary antibodies for 1 h at room temperature. Nuclei were labeled with DAPI and slides were covered with fluorescent mounting medium (F6057, Sigma). The primary antibodies used here were rabbit anti-insulin (1:200, ab63820, Abcam), mouse anti-glucagon (1:200, G2654, Sigma), rat anti-C-peptide (1:100, GN-ID4, University of Iowa Developmental Hybridoma Bank), and goat anti-PDX-1 (1:200, AF2419, R&D systems). The secondary antibodies used here are donkey anti-rabbit IgG AF488 (1:400, A21206, Thermofisher), donkey anti-rat IgG AF488 (1:400, A21208, Thermofisher), Texas Red horse anti mouse (1:200, TI-2000, Vector), and donkey anti-goat IgG AF594 (1:400, A11058, Thermofisher).

Scale-Up of SHIELD and Surgeries for Dog Studies: To facilitate the scale-up, SHIELD was adapted to the form of hanging-suture devices. Specifically, a nylon suture and a device with the desired length were bonded together by thermo sealing (Figure 7b). In addition, the thermo

bonding area and suture were coated with PDMS to mitigate tissue adhesion. The outer nanofibrous tube for hanging suture devices (length ≈ 12 cm, ID 3.2 mm) was coated by the in-out crosslinking method with 4% modified alginate (3:7). The inner nanofibrous tube (length ≈ 11 cm, OD ≈ 2.2 mm) was coated with 480 µL 2% SLG100 and inserted into the coated outer nanofibrous tube with the assistance of a stainless-steel capillary. A nylon template (11 cm × 2.5 mm × 0.25 mm) was inserted into the inner tube to prevent kinking. It should be noted that other plastic membranes with similar stiffness to nylon could also be used as the template to prevent kinking. Except for the abovementioned procedures, the fabrication process was the same as the rodent-size SHIELD. Long devices without a hanging suture (length ≈ 12 cm, ID 3.2 mm) were fabricated with a similar procedure.

Both implantation and retrieval were performed by laparoscopic surgeries. Before implantation, the intraperitoneal space was filled with CO_2 (10 mm Hg) to create enough space for surgical operation. Each device was placed in a plastic tube (≈10 mm in diameter) and delivered through a laparoscopic trocar by pushing with an aluminum rod. The devices were implanted near the urinary bladder. For the hanging-suture SHIELD, the suture end was grasped within the abdomen with a transperitoneal PMI Suture Grasper (OD 2.1 mm, Progressive Medical, Inc.), and the suture was fixed to the external fascia of the recipient's body wall. During retrieval, mild omentum adhesions were separated by electrocautery. Then the devices were pulled out through a laparoscopic trocar.

Statistical Analysis: Results were presented as mean ± standard deviation. Statistical analysis was conducted using GraphPad Prism 8.0.1. Unpaired *t*-test was performed when two groups were compared, while one-way ANOVA with a Tukey's multiple comparisons test was performed when more than two groups were compared. Statistical significance was determined as n.s., *, **, ***, ****, when the *p*-value was >0.05, <0.05, <0.01, <0.001, <0.0001, respectively.

Supporting Information

Supporting Information is available from the Wiley Online Library or from the author.

Acknowledgements

This work was mainly sponsored by Novo Nordisk Company and partially supported by the National Institutes of Health (NIH, 1R01DK105967-01A1), the Hartwell Foundation, and the Juvenile Diabetes Research Foundation (JDRF, 2-SRA-2018-472-S-B). The authors thank Cornell University Animal Health Diagnostic Center for histological sectioning and staining and acknowledge the use of field emission scanning electron microscopy from Cornell Center for Materials Research Shared Facilities (NSF MRSEC program, DMR-1719875). The authors also acknowledge the help on fabricating thermo cutting device from Fabio De Ferrari and helpful discussions from Tung Pham Thanh.

Conflict of Interest

W.L., M.M., J.A.F., L.-H.W., D.T.B., and Q.L. are inventors for a patent related to this manuscript.

Author Contributions

W.L. and M.M. conceived, designed the experiments, and wrote the manuscript. W.L. conducted the experiments and data analysis. J.A.F., W.L., L.H.W., and D.G. performed the dog experiments. L.H.W., K.S., and W.L. drew the schematics. Q.L. and D.T.B contributed to the device development. K.W. and X. W. conducted the immunohistochemical experiments. A.C. conducted a portion of the mouse experiments. J.C., B.P., K.S., and M.P. performed partial experiments and data collection. C.R., L.G.G., R.P.C., and L.W. contributed to the experiments for human SC-β cells. All authors discussed the results and contributed to the manuscript preparation.

Data Availability Statement

The data that support the findings of this study are available from the corresponding author upon reasonable request.

Keywords

cell encapsulation, cellular overgrowth, retrievability, scalability, type 1 diabetes

Received: October 5, 2021
Revised: November 12, 2021
Published online:

[1] D. W. Scharp, P. Marchetti, *Adv. Drug Deliver Rev.* **2014**, *67–68*, 35.
[2] a) T. Desai, L. D. Shea, *Nat. Rev. Drug Discovery* **2017**, *16*, 338; b) O. Veiseh, B. C. Tang, K. A. Whitehead, D. G. Anderson, R. Langer, *Nat. Rev. Drug Discovery* **2015**, *14*, 45.
[3] A. Katsarou, S. Gudbjörnsdottir, A. Rawshani, D. Dabelea, E. Bonifacio, B. J. Anderson, L. M. Jacobsen, D. A. Schatz, Å. Lernmark, *Nat. Rev. Dis. Primers* **2017**, *3*, 17016.
[4] A. U. Ernst, D. T. Bowers, L.-H. Wang, K. Shariati, M. D. Plesser, N. K. Brown, T. Mehrabyan, M. Ma, *Adv. Drug Deliver Rev.* **2019**, *139*, 116.
[5] D. T. Bowers, W. Song, L.-H. Wang, M. Ma, *Acta Biomater.* **2019**, *95*, 131.
[6] J. Yu, Y. Zhang, Y. Ye, R. DiSanto, W. Sun, D. Ranson, F. S. Ligler, J. B. Buse, Z. Gu, *Proc. Natl. Acad. Sci. U. S. A.* **2015**, *112*, 8260.
[7] a) B. Kovatchev, S. Anderson, L. Heinemann, W. Clarke, *Diabetes Care* **2008**, *31*, 1160; b) S. J. Russell, F. H. El-Khatib, M. Sinha, K. L. Magyar, K. McKeon, L. G. Goergen, C. Balliro, M. A. Hillard, D. M. Nathan, E. R. Damiano, *N. Engl. J. Med.* **2014**, *371*, 313.
[8] A. J. Shapiro, M. Pokrywczynska, C. Ricordi, *Nat. Rev. Endocrinol.* **2017**, *13*, 268.
[9] a) A. J. Shapiro, J. R. Lakey, E. A. Ryan, G. S. Korbutt, E. Toth, G. L. Warnock, N. M. Kneteman, R. V. Rajotte, *N. Engl. J. Med.* **2000**, *343*, 230; b) A. M. Posselt, M. D. Bellin, M. Tavakol, G. L. Szot, L. A. Frassetto, U. Masharani, R. K. Kerlan, L. Fong, F. G. Vincenti, B. J. Hering, J. A. Bluestone, P. G. Stock, *Am. J. Transplant.* **2010**, *10*, 1870; c) F. B. Barton, M. R. Rickels, R. Alejandro, B. J. Hering, S. Wease, B. Naziruddin, J. Oberholzer, J. S. Odorico, M. R. Garfinkel, M. Levy, *Diabetes Care* **2012**, *35*, 1436; d) E. A. Ryan, B. W. Paty, P. A. Senior, D. Bigam, E. Alfadhli, N. M. Kneteman, J. R. Lakey, A. M. James Shapiro, *Diabetes* **2005**, *54*, 2060.
[10] P. A. Senior, T. Kin, J. Shapiro, A. Koh, *Can. J. Diabetes* **2012**, *36*, 32.
[11] a) G. Orive, R. M. Hernández, A. R. Gascón, R. Calafiore, T. M. Chang, P. De Vos, G. Hortelano, D. Hunkeler, I. Lacík, A. M. James Shapiro, *Nat. Med.* **2003**, *9*, 104; b) G. Orive, E. Santos, D. Poncelet, R. M. Hernández, J. L. Pedraz, L. U. Wahlberg, P. De Vos, D. Emerich, *Trends Pharmacol. Sci.* **2015**, *36*, 537.
[12] a) A. Veres, A. L. Faust, H. L. Bushnell, E. N. Engquist, J. H.-R. Kenty, G. Harb, Y.-C. Poh, E. Sintov, M. Gürtler, F. W. Pagliuca, Q. P. Peterson, D. A. Melton, *Nature* **2019**, *569*, 368; b) N. Sharon, R. Chawla, J. Mueller, J. Vanderhooft, L. J. Whitehorn, B. Rosenthal, M. Gürtler, R. R. Estanboulieh, D. Shvartsman, D. K. Gifford, C. Trapnell, D. Melton, *Cell* **2019**, *176*, 790; c) F. W. Pagliuca,

J. R. Millman, M. Gürtler, M. Segel, A. Van Dervort, J. H. Ryu, Q. P. Peterson, D. Greiner, D. A. Melton, *Cell* **2014**, *159*, 428; d) A. Rezania, J. E. Bruin, P. Arora, A. Rubin, I. Batushansky, A. Asadi, S. O'dwyer, N. Quiskamp, M. Mojibian, T. J. N. b. Albrecht, *Nat. Biotechnol.* **2014**, *32*, 1121; e) T. Guo, L. Landsman, N. Li, M. J. D. Hebrok, *Diabetes* **2013**, *62*, 1581; f) D. Van Hoof, A. D. Mendelsohn, R. Seerke, T. A. Desai, M. S. J. S. c. r. German, *Stem Cell Res.* **2011**, *6*, 276; g) N. J. Hogrebe, P. Augsornworawat, K. G. Maxwell, L. Velazco-Cruz, J. R. J. N. b. Millman, *Nat. Biotechnol.* **2020**, *38*, 460; h) K. G. Maxwell, P. Augsornworawat, L. Velazco-Cruz, M. H. Kim, R. Asada, N. J. Hogrebe, S. Morikawa, F. Urano, J. R. J. S. t. m. Millman, *Sci. Transl. Med.* **2020**, *12*, eaax9106; i) G. G. Nair, J. S. Liu, H. A. Russ, S. Tran, M. S. Saxton, R. Chen, C. Juang, M.-l. Li, V. Q. Nguyen, S. J. N. c. b. Giacometti, *Nat. Cell Biol.* **2019**, *21*, 263.

[13] a) R. Chang, G. Faleo, H. A. Russ, A. V. Parent, S. K. Elledge, D. A. Bernards, J. L. Allen, K. Villanueva, M. Hebrok, Q. Tang, *ACS Nano* **2017**, *11*, 7747; b) J. M. Anderson, A. Rodriguez, D. T. Chang, *Semin. Immunol.* **2008**, *20*, 86; c) J. L. Harding, M. M. J. T. i. b. Reynolds, *Trends Biotechnol.* **2014**, *32*, 140; d) D. W. J. N. b. Grainger, *Nat. Biotechnol.* **2013**, *31*, 507; e) D. F. J. B. Williams, *Biomaterials* **2008**, *29*, 2941; f) G. Wick, C. Grundtman, C. Mayerl, T.-F. Wimpissinger, J. Feichtinger, B. Zelger, R. Sgonc, D. J. A. r. o. i. Wolfram, *Annu. Rev. Immunol.* **2013**, *31*, 107; g) T. A. Wynn, T. R. J. N. m. Ramalingam, *Nat. Med.* **2012**, *18*, 1028; h) Q. Xu, A. S. , Y. Gao, L. Guo, J. Creagh-Flynn, D. Zhou, U. Greiser, Y. Dong, F. Wang, H. Tai, W. Liu, W. Wang, W. Wang, *Acta Biomater.* **2018**, *75*, 63.

[14] S. Bose, L. R. Volpatti, D. Thiono, V. Yesilyurt, C. McGladrigan, Y. Tang, A. Facklam, A. Wang, S. Jhunjhunwala, O. Veiseh, J. Hollister-Lock, C. Bhattacharya, G. C. Weir, D. L. Greiner, R. Langer, D. G. Anderson, *Nat. Biomed. Eng.* **2020**, *4*, 814.

[15] a) M. Kumagai-Braesch, S. Jacobson, H. Mori, X. Jia, T. Takahashi, A. Wernerson, M. Flodström-Tullberg, A. J. C. t. Tibell, *Cell Transplant.* **2013**, *22*, 1137; b) C. Haller, J. Piccand, F. De Franceschi, Y. Ohi, A. Bhoumik, C. Boss, U. De Marchi, G. Jacot, S. Metairon, P. J. S. c. r. Descombes, *Stem Cell Rep.* **2019**, *12*, 787.

[16] a) B. Ludwig, B. Zimerman, A. Steffen, K. Yavriants, D. Azarov, A. Reichel, P. Vardi, T. German, N. Shabtay, A. J. H. Rotem, M. Research, *Horm. Metab. Res.* **2010**, *42*, 918; b) U. Barkai, G. C. Weir, C. K. Colton, B. Ludwig, S. R. Bornstein, M. D. Brendel, T. Neufeld, C. Bremer, A. Leon, Y. J. C. t. Evron, *Cell Transplant.* **2013**, *22*, 1463.

[17] L. C. Pullen, *Am. J. Transplant.* **2018**, *18*, 1581.

[18] Q. Liu, A. Chiu, L.-H. Wang, D. An, M. Zhong, A. M. Smink, B. J. de Haan, P. de Vos, K. Keane, A. Vegge, *Nat. Commun.* **2019**, *10*, 1.

[19] H. Hentze, P. L. Soong, S. T. Wang, B. W. Phillips, T. C. Putti, N. R. J. S. c. r. Dunn, *Stem Cell Res.* **2009**, *2*, 198.

[20] a) E. Dolgin, *Nat. Med.* **2014**, *20*, 9; b) O. Veiseh, J. C. Doloff, M. Ma, A. J. Vegas, H. H. Tam, A. R. Bader, J. Li, E. Langan, J. Wyckoff, W. S. Loo, S. Jhunjhunwala, A. Chiu, S. Siebert, K. Tang, J. Hollister-Lock, S. Aresta-Dasilva, M. Bochenek, J. Mendoza-Elias, Y. Wang, M. Qi, D. M. Lavin, M. Chen, N. Dholakia, R. Thakrar, I. Lacík, G. C. Weir, J. Oberholzer, D. L. Greiner, R. Langer, D. G. Anderson, *Nat. Mater.* **2015**, *14*, 643; c) K. Y. Lee, D. J. Mooney, *Prog. Polym. Sci.* **2012**, *37*, 106; d) C. J. Kearney, D. J. J. N. m. Mooney, *Nat. Mater.* **2013**, *12*, 1004.

[21] A. J. Vegas, O. Veiseh, J. C. Doloff, M. Ma, H. H. Tam, K. Bratlie, J. Li, A. R. Bader, E. Langan, K. Olejnik, P. Fenton, J. W. Kang, J. Hollister-Locke, M. A. Bochenek, A. Chiu, S. Siebert, K. Tang, S. Jhunjhunwala, S. Aresta-Dasilva, N. Dholakia, R. Thakrar, T. Vietti, M. Chen, J. Cohen, K. Siniakowicz, M. Qi, J. McGarrigle, S. Lyle, D. M. Harlan, D. L. Greiner, J. Oberholzer, G. C. Weir, R. Langer, D. G. Anderson, *Nat. Biotech.* **2016**, *34*, 345.

[22] D. An, A. Chiu, J. A. Flanders, W. Song, D. Shou, Y.-C. Lu, L. G. Grunnet, L. Winkel, C. Ingvorsen, N. S. Christophersen, *Proc. Natl. Acad. Sci. U. S. A.* **2017**, *115*, E263.

[23] A. J. Vegas, O. Veiseh, M. Gürtler, J. R. Millman, F. W. Pagliuca, A. R. Bader, J. C. Doloff, J. Li, M. Chen, K. Olejnik, H. H. Tam, S. Jhunjhunwala, E. Langan, S. Aresta-Dasilva, S. Gandham, J. J. McGarrigle, M. A. Bochenek, J. Hollister-Lock, J. Oberholzer, D. L. Greiner, G. C. Weir, D. A. Melton, R. Langer, D. G. Anderson, *Nat. Med.* **2016**, *22*, 306.

[24] a) S. Jiang, Z. J. A. m. Cao, *Adv. Mater.* **2010**, *22*, 920; b) J. Ladd, Z. Zhang, S. Chen, J. C. Hower, S. J. B. Jiang, *Biomacromolecules* **2008**, *9*, 1357; c) L. Zhang, Z. Cao, T. Bai, L. Carr, J. R. Ella-Menye, C. Irvin, B. D. Ratner, S. Jiang, *Nat. Biotechnol.* **2013**, *31*, 553.

[25] M. A. Bochenek, O. Veiseh, A. J. Vegas, J. J. McGarrigle, M. Qi, E. Marchese, M. Omami, J. C. Doloff, J. Mendoza-Elias, M. Nourmohammadzadeh, A. Khan, C.-C. Yeh, Y. Xing, D. Isa, S. Ghani, J. Li, C. Landry, A. R. Bader, K. Olejnik, M. Chen, J. Hollister-Lock, Y. Wang, D. L. Greiner, G. C. Weir, B. L. Strand, A. M. A. Rokstad, I. Lacik, R. Langer, D. G. Anderson, J. Oberholzer, *Nat. Biomed. Eng.* **2018**, *2*, 810.

[26] a) K. Y. Lee, D. J. Mooney, *Chem. Rev.* **2001**, *101*, 1869; b) A. Khademhosseini, R. J. B. Langer, *Biomaterials* **2007**, *28*, 5087.

[27] J. A. Steele, J.-P. Hallé, D. Poncelet, R. J. A. d. d. r. Neufeld, *Adv Drug Deliver Rev* **2014**, *67*, 74.

[28] D. An, Y. Ji, A. Chiu, Y.-C. Lu, W. Song, L. Zhai, L. Qi, D. Luo, M. Ma, *Biomaterials* **2015**, *37*, 40.

[29] X. Wang, K. Wang, W. Zhang, M. Qiang, Y. Luo, *Biomaterials* **2017**, *138*, 80.